SANDIA REPORT

SAND2004-5309
Unlimited Release
Printed December 2004

Evaluation of Ingredients for the Development of New Insensitive Munitions

Richard Behrens, Deneille Wiese-Smith, Lois Johnston and Sean Maharrey,

Prepared by
Sandia National Laboratories
Albuquerque, New Mexico 87185 and Livermore, California 94550

Sandia is a multiprogram laboratory operated by Sandia Corporation,
a Lockheed Martin Company, for the United States Department of Energy's
National Nuclear Security Administration under Contract DE-AC04-94-AL85000.

Issued by Sandia National Laboratories, operated for the United States Department of Energy by Sandia Corporation.

Available to DOE and DOE contractors from
U.S. Department of Energy
Office of Scientific and Technical Information
P.O. Box 62
Oak Ridge, TN 37831

Telephone: (865) 576-8401
Facsimile: (865) 576-5728
E-Mail: reports@adonis.osti.gov
Online ordering: http://www.doe.gov/bridge

Available to the public from
U.S. Department of Commerce
National Technical Information Service
5285 Port Royal Rd
Springfield, VA 22161

Telephone: (800) 553-6847
Facsimile: (703) 605-6900
E-Mail: orders@ntis.fedworld.gov
Online order: http://www.ntis.gov/help/ordermethods.asp?loc=7-4-0#online

SAND2004-5309
Unlimited Release
Printed December 2004

Evaluation of Ingredients for the Development of New Insensitive Munitions

Richard Behrens, Deneille Wiese-Smith, Lois Johnston and Sean Maharrey,
Combustion Research Facility
Sandia National Laboratories
P.O. Box 969
Livermore, California 94551-0969

ABSTRACT

Several ingredients being considered by the U.S. Army for the development of new insensitive munitions have been examined. One set of ingredients consists of 2,4-dinitrophenylhydrazine (DNPH) and hexahydro-1,3,5-trinitro-s-triazine (RDX). In this set, the decomposition of the mixture was examined to determine whether adding DNPH to RDX would generate a sufficient quantity of gas to rupture the case of a munition prior to the onset of the rapid reaction of RDX, thus mitigating the violence of reaction. The second set of ingredients consists of three different reduced sensitivity RDX (RS-RDX) powders manufactured by SNPE and Dyno-Nobel. In this set, the objective was to determine properties of RS-RDX powders that may distinguish them from normal RDX powder and may account for their reduced shock sensitivity.

The decomposition reactions and sublimation properties of these materials were examined using two unique instruments: the simultaneous thermogravimetric modulated beam mass spectrometry (STMBMS) instrument and the Fourier Transform ion cyclotron resonance (FTICR) mass spectrometry instrument. These instruments provide the capability to examine the details of decomposition reactions in energetic materials.

DNPH does not appear to be a good candidate to mitigate the violence of the RDX reaction in a munition. DNPH decomposes between 170°C and 180°C. When mixed with RDX it decomposes between 155°C and 170°C. It decomposes to form 1,3-dintrobenzene (DNB), ammonia, water and nitrogen. Of these compounds only nitrogen and ammonia are capable of generating high pressures within a munition. When DNPH is mixed with RDX, the DNB formed in the decomposition of DNPH interacts with RDX on the surface of the RDX powder leading to a higher rate of formation of CH_2O and N_2O. The CH_2O is consumed by reaction with DNPH to form 2-methylene-1-(2,4-dintrophenyl)hydrazine. As a result, DNPH does not generate a large quantity of gas that will lead to rupture of a munition case. Another compound to consider as an additive is 2-oxo-1,3,5-trinitro-1,3,5-triazacyclohexane (K-6), which generates more gas in the required temperature range.

Examination of several different RS-RDX materials has shown that their sublimation rates and decomposition behavior differ from Holston grade RDX. The results suggest that insensitive RDX materials from both SNPE and Dyno-Nobel may have a shell-like structure of RDX on the surface of the particles that is less stable and more reactive than the material in the core of the particles. The origin of this shell-like RDX structure is uncertain, but may be due to some aspect of the manufacturing process. It is possible that this less stable RDX on the surface of the particles may be more fluid than the interior of the particles, allowing more slip between the surface of the particles under impact or shock. This may play a role in the reduced shock sensitivity of the insensitive RDX materials.

The results of over 50 experiments with DNPH, mixtures of DNPH and RDX and insensitive RDX are presented. The results characterize the decomposition behavior of each of these materials.

CONTENTS

Abstract 3
Contents 5
Tables 6
Introduction 7
Experimental Methods 8
The STMBMS apparatus. 8
Mass spectrometry measurements. 9
Vapor pressure measurements. 10
Sample preparation 10
Results – General Information 13
DNPH Results 14
2,4-Dinitrophenyl hydrazine (DNPH) 14
  Mass spectra. 14
  Vapor pressure. 14
  Contaminants in DNPH 15
  Thermal Decomposition. 15
    Ion Signals 15
    Autocatalysis 17
    Rapid Heating/DSC Comparison 19
    DNPH Summary 20
Decomposition of DNPH and RDX Mixtures 20
    Ion Signals 21
    Effects on DNPH 21
    Effects on RDX 22
    Changing Confinement 23
    DNPH and IRDX Mixtures 24
Insensitive RDX 27
  Insensitive RDX. 27
  RDX vapor pressure results. 27
  RDX decomposition results. 29
    ONDNTA reaction pathway. 32
Discussion 34
Conclusions 37
Acknowledgements 38
Bibliography 38

Appendix 41
Distribution 63

TABLES

Table. 1. DNPH and RDX samples 11
Table. 2. Experiments with DNPH 42
Table. 3. Experiments with RDX 44
Table. 4. Experiments with Mixtures of DNPH and RDX 48
Table. 5. High Resolution Spectra of DNPH 53
Table. 6. High Resolution Spectra from the Decomposition of DNPH. 55
Table. 7. High Resolution Spectra from the Decomposition of DNPH and RDX. 59

Evaluation of Ingredients for the Development of New Insensitive Munitions

Introduction

DoD requires that all new munitions placed into service meet insensitive munition requirements. To meet these requirements the U.S.Army Tank-automotive and Armaments Command (TACOM) at the Armament Research, Development and Engineering Center (ARDEC) is investigating new methods to design munitions that meet the requirements for insensitivity. One approach is to utilize a new type of RDX, which appears to be less sensitive than RDX manufactured at the Holston Defense Plant and used in almost all munitions. Another approach is to explore the feasibility of developing new insensitive munitions by adding special ingredients to explosive formulations. In this approach the concept is to add ingredients that will decompose at lower temperatures than the energetic ingredients and burst the confining case prior to the onset of a violent cookoff event caused by reaction of the energetic ingredients, such as RDX or TNT.

Reduced sensitivity RDX (RS-RDX), manufactured by SME Groupe SNPE and Dyno-Nobel, has been examined by TACOM for use in new munitions. Tests with the new RS-RDX show that these materials have lower shock sensitivity than normal RDX. However, it has been difficult to characterize the specific properties of these materials that lead to their decreased sensitivity, making it difficult to develop a set of material specifications needed for procurement.

Different additives were investigated at ARDEC to mitigate the violence of reaction of TNT. Initial work in which PETN was added to TNT showed encouraging results. These tests were then expanded to include melt cast explosives, such as Comp B (63% RDX, 36% TNT, 1% wax).[1] After tests with Comp B, PETN was removed from consideration and a search was made for other additives. Through a contract with ATK Thiokol Propulsion, one additive, 2,4-dinitrophenyl hydrazine (DNPH), was found to reduce the violence of reactions and was selected for further study at ARDEC.

The program at ARDEC is currently focused on evaluating the effects of various ingredients on violence of response in TNT, Comp B, and PAX/AFX 194. PAX/AFX 194 is an explosive made from an HMX-free RDX and an inert binder. This explosive formulation is of interest for future munitions, since TNT may no longer be available for use in new munitions and thus it may not be possible to utilize Comp B in new munitions.

In evaluating ingredients to mitigate cookoff violence three general issues must be addressed:

1. The decomposition behavior of the additives and how it relates to and influences the behavior of the energetic ingredients.
2. The long-term compatibility of the additives and the energetic ingredients.
3. Effects of aging on the ability of the additives to mitigate cookoff violence.

The underlying phenomena of each issue must be understood before moving on to larger scale tests of the more promising formulations.

The objective of this project is to support the ARDEC program that is focused on the development of new insensitive munitions whose violent response is mitigated by the addition of additives to the explosive formulation. The general concept envisions the addition of chemical additives that undergo reaction prior to the main explosive and lead to a mild rupture of the confining case, resulting in the

deflagration of the remaining energetic ingredients. The target explosives for the ARDEC study are RDX, TNT and Comp B. The additive that is currently being investigated by ARDEC is DNPH. Since the Army is phasing out the use of TNT, our study focuses on the use of additives to mitigate the violence of RDX-based explosives.

To address the three general issues, thermal decomposition studies of DNPH, RDX and mixtures of DNPH and RDX have been carried out using Sandia's simultaneous thermogravimetric modulated beam mass spectrometry (STMBMS) apparatus and a Fourier Transform ion cyclotron resonance (FTICR) mass spectrometer. The objectives of these experiments are to 1) characterize the decomposition behavior of DNPH, 2) characterize the decomposition behavior of RS-RDX, and 3) characterize the interactions of DNPH and RDX during the thermal decomposition process.

To characterize the decomposition behavior of DNPH the following data have been collected: mass spectra, vapor pressure, evolution of contaminants, and the thermal decomposition behavior under low and high confinement conditions.

To characterize the thermal decomposition of the new RS-RDX materials a limited number of thermal decomposition experiments with these materials in the solid phase have been conducted and the results are compared to our previous studies with high purity RDX and RDX manufactured at the Holston Defense plant. The results provide new insight into differences in the properties of RS-RDX and RDX that may account for the insensitive nature of the new materials.

To characterize the interactions of DNPH with RDX, a series of thermal decomposition experiments have been conducted with physical mixtures of the RDX and DNPH powders. These experiments have focused on assessing the degree of decomposition of each component in the presence of the other and the degree of synergistic interactions between the ingredients. The results have shown that DNPH may not be a suitable candidate because the low vapor pressure of the gases evolving in the reactions makes rupture of a confining case unlikely.

Three important conclusions have been derived from this study. First, the STMBMS methods provide a unique means of evaluating the reaction processes that occur between ingredients being considered for new explosive or propellant formulations. Second, insensitive forms of RDX may have a layer of material on the surface of the particles whose properties differ from those of the core of the particles and may account for the reduced shock sensitivity of these materials. Third, the addition of DNPH to RDX is not likely to mitigate the violence of reaction of RDX because decomposition of the DNPH does not generate a sufficient amount of gaseous products to rupture the case of a munition prior to the onset of a violent cookoff event. The report presents a brief description of the experimental methods, the results from experiments with DNPH, RS-RDX and mixtures of RDX and DNPH and the conclusions drawn from the current set of experiments.

Experimental Methods

The STMBMS apparatus.

The simultaneous thermogravimetric modulated beam mass spectrometry (STMBMS) apparatus, and basic experimental and data analysis procedures have been described previously.[2-4] A schematic diagram of the instrument is shown in Figure 1. This instrument allows the concentration and rate of formation of each gas-phase species in a reaction cell to be measured as a function of time by correlating the ion signals at different m/z values measured with a mass spectrometer with the force measured by a microbalance at any instant. In an experiment, a small sample (~10 mg) is placed in an alumina reaction cell. The reaction cell is then mounted on a thermocouple probe that is seated in

a microbalance. The reaction cell is enclosed in a high vacuum environment (< 10^{-6} Torr) and is radiatively heated by a bifilar-wound tantalum wire on an alumina tube.

The molecules from the gaseous mixture in the reaction cell exit through a small diameter orifice (2.5 to 970 µm, orifice length is 25 µm) in the cap of the reaction cell, traverse two beam-defining orifices before entering the electron-bombardment ionizer of the mass spectrometer. The ions are created by collisions of 20 eV electrons with the different molecules in the gas flow. A relatively low electron energy of 20 eV (compared to 70 eV used on normal mass spectrometry measurements) is used to reduce the extent of fragmentation of the higher molecular weight ions and, thus, limit their contribution to ion signals measured at lower m/z values that are associated with the thermal decomposition products.

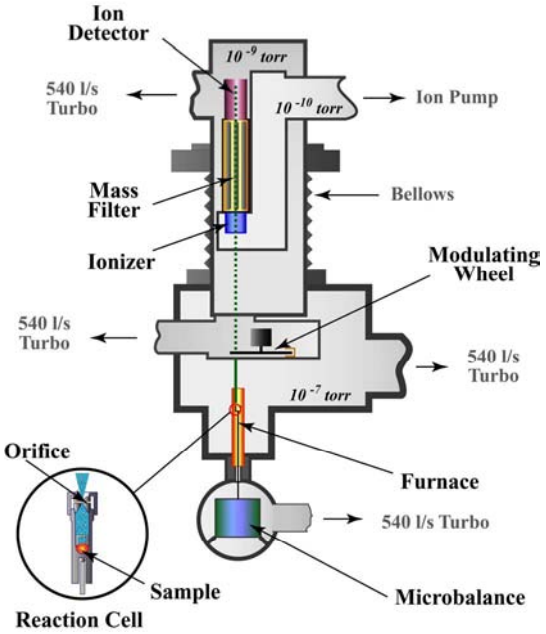

Figure 1. Schematic cross section of STMBMS apparatus.

The background pressures in the vacuum chambers are sufficiently low to eliminate significant scattering between molecules evolving from the reaction cell and background molecules in the vacuum chambers, thus enabling the gas evolving from the reaction cell to be sampled directly by the mass spectrometer. The different m/z-value ions are selected with a quadrupole mass filter and counted with an ion counter. The gas flow is modulated with a chopping wheel and only the modulated ion signal is recorded.

The containment time of gas in the reaction cell is a function of the orifice area, the free volume within the reaction cell, and the characteristics of the flow of gas through the orifice. The time constant for the rate of gas leaving the cell depends on the orifice diameter and ranges from ~ 50 sec for the 5 µm diameter orifices to less than < 0.1 sec for the 970 µm diameter orifices. These times are short compared to the duration of the experiments (>1000 sec). The pressure of the gaseous products within the reaction cell range from less that 1 Torr for experiments with the larger diameter orifices (970µm) to greater than 1000 Torr for experiments with the smallest diameter orifices (2.5µm).

Mass spectrometry measurements.

The mass spectra are measured with two different instruments. The STMBMS apparatus is used to collect low-resolution mass spectra by heating the sample in the reaction cell to temperatures that generate a sufficient amount of vapor but do not cause decomposition. Larger diameter orifices (~ 1000 µm) are used to reduce the required temperature. A Fourier Transform ion cyclotron resonance (FTICR) mass spectrometer is used to collect high resolution ($m/\Delta m$ > 50,000) and high mass accuracy (< 1 ppm) mass spectra. This data is used to assign the stoichiometry of the ions in the mass spectra.

To identify the decomposition products, samples of the partially decomposed compounds are prepared by placing the sample in glass capillary tube, loading the capillary tubes into the reaction cell and decomposing the sample in the STMBMS apparatus until a desired point in the decomposition process is obtained. At this point the sample is cooled and the capillary tubes, containing the partially decomposed sample, are removed for analysis with the FTICR mass

spectrometer. The samples are slowly heated in the direct insertion probe of the FTICR mass spectrometer to obtain the spectra of the decomposition products.

The stoichiometries of the individual ions are assigned from the high mass accuracy data obtained with the FTICR mass spectrometer. The association of ions at individual m/z values with the reactant or compound formed in the decomposition process is determined from a correlation analysis of the time-dependent ion signals measured in the STMBMS experiments and the FTICR spectra.

Vapor pressure measurements.

The vapor pressures of the compounds are measured with the STMBMS apparatus. In these experiments the sample is placed in a reaction cell that is fitted with a larger diameter orifice (typically, 0.25 to 1.0 mm). The sample is heated through a set of isothermal temperature steps and the mass spectra and rate of force change are measured with the STMBMS apparatus. The data is analyzed with the STMBMS thermal analysis algorithms and the vapor pressure of the compound at each temperature step is determined. The measurements are typically obtained by collecting data in a series of increasing temperature steps followed by a series of decreasing temperature steps. These two sets of isothermal data are compared and used to check for the evolution of volatile contaminants from the samples that may influence the initial vapor pressure measurements.

The vapor pressures are measured over a temperature range in which molecular flow controls the rate of mass loss from the reaction cell (Knudsen number > 10). The mass loss is described by the following expression

$$\frac{dm}{dt} = \frac{C A_0 M \bar{v}(t) n(t)}{4 N_A}$$

where C is the Clausing factor, A_0 is the area of the orifice, N_A is Avagodro's number, M is the molecular weight, v is the average velocity of the gas, and n is the number density of the gas. The vapor pressures are related to the number density through the ideal gas law.

The vapor pressure measurements assume that equilibrium is maintained between the solid phase and gas phase. This condition is obtained if the surface area of the sample is much larger that the area of the exit orifice. For the larger diameter orifices (~1000 μm) this condition is not met and differences as large as a factor of 3 have been observed. However, the results presented in this report have been collected using orifices of nominally the same size, so that relative comparisons between different materials can be made.

Sample preparation.

The DNPH was obtained from two sources: Arcos Chemicals (sample DNPH01) and Alpha Asar (supplied by U.S Army TACOM, sample DNPH02). Both samples contain approximately 30% water by weight. The DNPH01 sample was dried by heating in a vacuum oven at 40°C for one hour. The DNPH02 sample was dried at Picatinny Arsenal by heating at 48.9°C until the sample stopped losing weight.

Four types of RDX samples are used in the experiments. One is manufactured at Holston Defense plant and has been used at Sandia. U.S Army TACOM supplied three additional samples.

1. Special processed Holston RDX manufactured ~ Sept. 2000, supplied by: SME Groupe SNPE, Etablissement de Sorgues, BP311, 84706 Sorgues Cedex, France.

2. SNPE IRDX material manufactured ~ Aug 2000, supplied by: SME Groupe SNPE, Etablissement de Sorgues, BP311, 84706 Sorgues Cedex, France.
3. Dyno-Nobel IRDX material manufactured July 2002 supplied by: Dyno Nobel ASA, P.O. Box 10, N-3476 Saetre, Norway.

Table. 1. DNPH and RDX samples

Sample	Manufacturer	RDX source	Year*	AKA
DNPH01	Arcos Chem.	-	2003	-
DNPH02	Alpha Asar	-	2002	-
RDX_01	Holston	Holston	<1985	A213
IRDX_01	SNPE	Holston	2000	HIRDX
IRDX_02	SNPE	SNPE	2000	SIRDX
IRDX_03	Dyno-Nobel	Dyno-Nobel??	2002	IRDX

* Year manufactured.

Results – General Information

Several types of experiments have been used to examine the thermal decomposition processes in DNPH, RDX and mixtures of these two materials. Over sixty experiments have been conducted during this study. Tables A-I, A-II, and A-III list the different experiments conducted with DNPH, RDX, and DNPH/RDX mixture, respectively. Three types of experiments provide the following information on each compound and / or mixture: (1) mass spectra, (2) vapor pressure, and (3) decomposition behavior at different temperatures, heating rates and pressures of the confined gaseous decomposition products.

This report utilizes results from selected experiments to illustrate the general findings of this study. Since our main objective was to understand the interactions of DNPH with RDX, this study presents the qualitative findings from our experiments on the interactions of the ingredients and not the detailed analysis of the data that can be used to construct models of the reactions kinetics of the ingredients for use in predictive models. For example, if it were found that the interaction of DNPH with RDX was a good candidate as an additive to mitigate reaction violence, then conducting a series of additional experiments could yield details of the reaction kinetics that control the decomposition of DNPH and its interaction with RDX. This information could be useful in larger scale codes that account for thermal and mass transport, where the response of a munition could be modeled under various cookoff scenarios. Since the initial results indicate the DNPH is not a good candidate as an ingredient to mitigate the violence of reaction, a qualitative understanding of the reaction processes was sufficient for this investigation.

Results that illustrate the decomposition processes in DNPH and DNPH/RDX mixtures are presented first. Next, results on the surface properties of the insensitive RDX materials are presented. The experimental conditions for the selected experiments, as denoted by the experiment names in the text, may be found in Tables A-I, A-II, and A-III.

DNPH Results

2,4-Dinitrophenyl hydrazine (DNPH)

Mass spectra.

The m/z values and formulas of the ions that comprise the mass spectra of DNPH are listed in Table B-I. The relative intensities of each ion listed were determined using the STMBMS instrument and an electron energy of 20 eV. The ion formulas were determined from the high accuracy mass measurements obtained with the FTICR mass spectrometer. In several cases, the high-resolution mass spectrum shows ions with different formulas that appear at the same nominal m/z value. These are listed in Table B-I.

Vapor pressure.

The vapor pressure of DNPH was measured between 70°C and 140°C using a 980µm orifice (DNPH003). A plot of the vapor pressure and a comparison to the vapor pressure of RDX (RDX282) is shown in Figure 2. The vapor pressure of DNPH is represented by the expression: $\log_{10} P$ (Torr)= 12.582 – 6480/T (K). The vapor pressure measurements before and after heating to 140°C were approximately the same, indicating that heating did not alter DNPH in a manner that affects its sublimation characteristics. The heat of sublimation of DNPH is 29.7 kcal/mol. The vapor pressure of DNPH is approximately a factor of five lower than RDX. (Note that these measurements were made with a large orifice, resulting in a vapor pressure that may be up to a factor of three below the

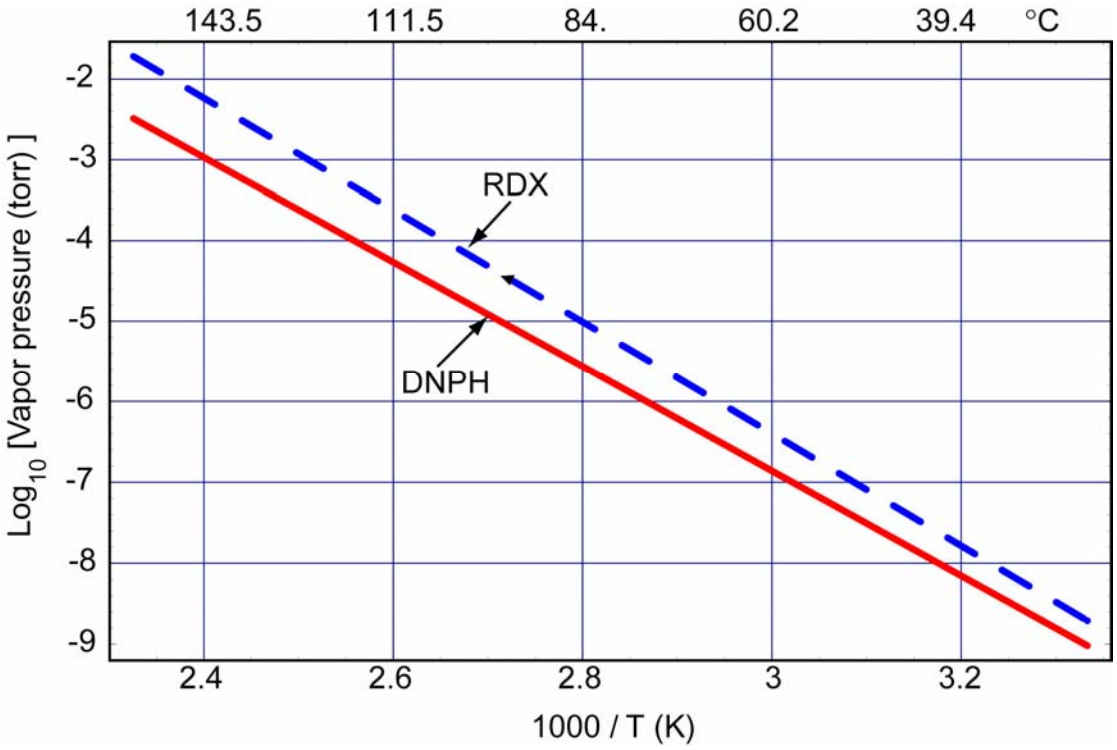

Figure 2. Vapor pressure of RDX and DNPH.

real vapor pressure value.)

Contaminants in DNPH.

Two different DNPH samples were heated in the STMBMS apparatus to determine the identities and quantities of contaminants contained in the DNPH sample. The water mixed with the samples was very volatile. In one experiment, a wet DNPH01 was examined with STMBMS apparatus. In this experiment the sample lost more than 99% of the water in the process of evacuating the apparatus, prior to collecting data.

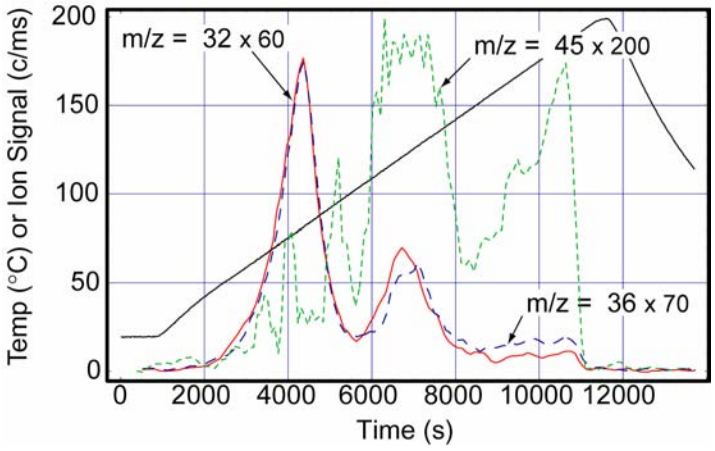

Figure 3. Ion signal from contaminants that evolve from DNPH01 as it is heated. The signals represent CH_3OH (32), HCl (36) and m/z=45. Data from experiment DNPH001.

The extent of contamination of the two DNPH samples differed. Several contaminants evolved from the DNPH01 sample as it was heated from 40°C to 160°C. Similar contaminants were not observed in the DNPH02 sample.

The contaminants that evolve from the DNPH01 sample are CH_3OH, HCl and a product with an ion signal at m/z=45 whose identity is unknown. Their rates of evolution as the sample is heated are shown in Figure 3. The multiple peaks observed in the evolution of each contaminant suggest that there are two different types of bonding to the DNPH.

Thermal Decomposition.

Ion Signals

The thermal decomposition of DNPH was examined with a series of experiments conducted under a range of thermal and sample confinement conditions.

The products are identified using data from the STMBMS and FTICR mass spectrometry instruments. The mass spectrometry data from the STMBMS instrument is sorted into temporally correlated groups as shown in Figure 4. The groups represent ion signals in the mass spectra that originate from either the same parent molecule or a set of parent molecules that have similar rates of formation in the decomposition process. Ions at m/z values that originate from one compound will have ion signals that are highly correlated in time, whereas ions at m/z values that originate from a set of compounds will have a lower correlation.

The ion signals shown in Fig. 4A have a high degree of correlation (0.98 to 1.0). These ion signals are associated with the main decomposition pathway of DNPH. The ion signals shown in Fig. 4B – 4D represent several other compounds that are formed during the decomposition process. These are minor products (as roughly indicated by their lower relative intensities), but may play a role as an "autocatalyst" as indicated by their early appearance and their persistence after the main reaction is complete. The ion signals shown in 4D are in a correlation band with a wider range (0.8 to 1.0) and originate from two different decomposition products.

To determine the formulas of the ions in each of the correlated groups, a sample is partially decomposed and cooled in the STMBMS instrument. The partially decomposed sample is then

transferred to the FTICR instrument where the sample is evaporated by heating the sample in a direct insertion probe (DIP). Mass spectra are recorded as a function of time as the sample is heated. The results are analyzed to determine the formula of the various ions in the mass spectra of the evolving mixture of compounds. The results are presented in Table B-II.

Combining the results from the STMBMS and FTICR measurements, the main products formed during the decomposition have been determined and are listed in Table II. The main decomposition products are m-dinitrobenzene (DNB), NH_3, H_2O and N_2. Two other products are observed that have

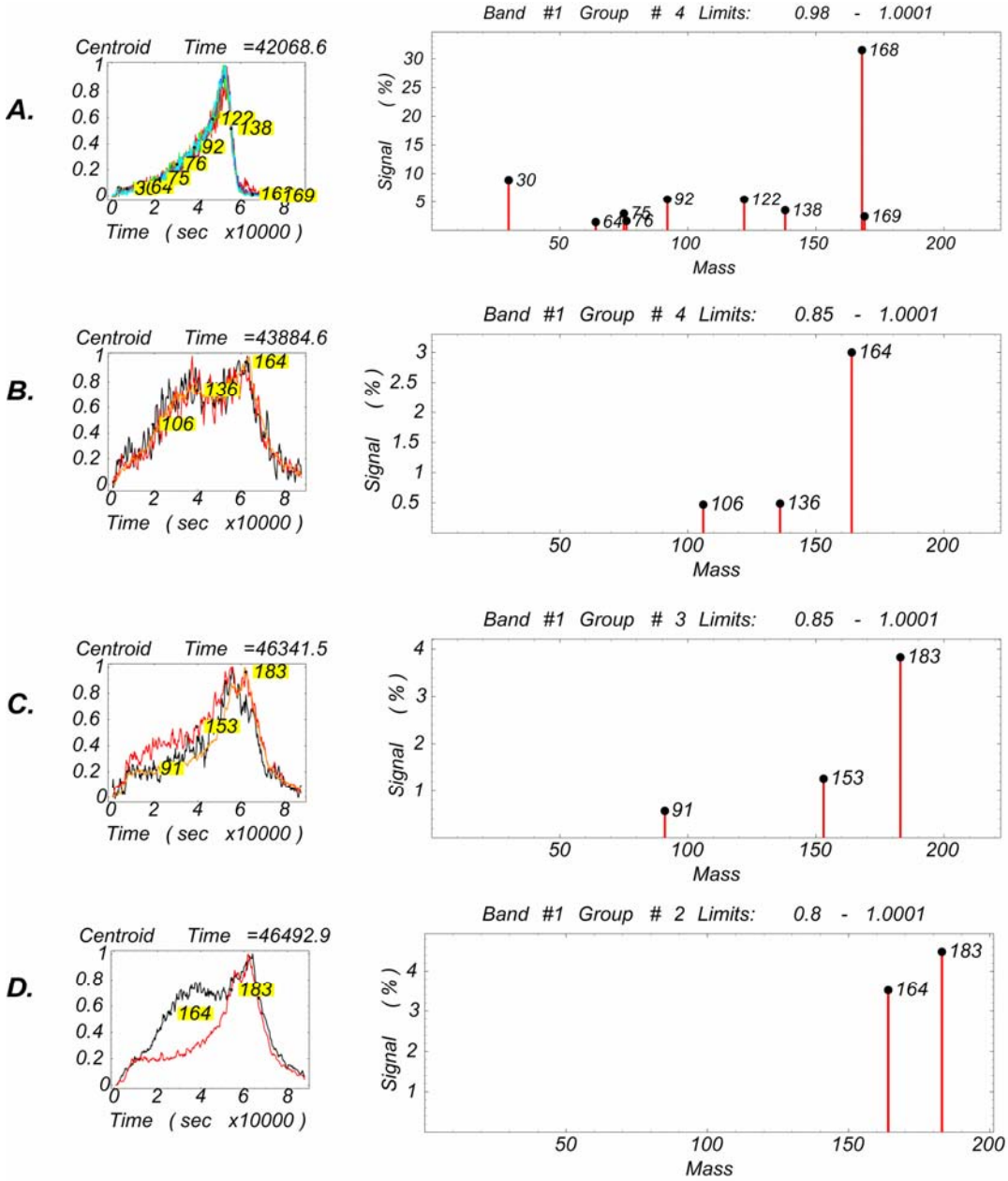

Figure 4. Groups of temporally correlated ion signals formed in the decomposition of DNPH (DNPH023). The graphs on the left show the temporal behavior of the various ion signals. The graphs on the right show the relative intensity of each signal in each group. The limits of the correlation band for each grouping are shown above the mass spectra.

a broad temporal behaviors as illustrated in Fig. 4. These products are 6-nitro-1,2,3 benzotriazole (164) (NBT) and 2,4-dinitro aniline (183) (DNA).

The ion signals formed from the compounds that evolve from a DNPH sample as it is heated at 3.3 °C/hr are shown in Fig. 5. At 140°C the ion signal (m/z=198) associated with DNPH increases as the vapor pressure rises with increasing temperature. This is followed by an increase in the signal (m/z=164) from NBT. At ~160°C the signal (m/z=183) from DNA starts to increase. At ~170°C the ion signals (m/z= 17, 18, 28, 168) from the main products formed during the decomposition of DNPH first appear.

Table II. Products formed in the decomposition of 2,4-Dinitrophenyl hydrazine.

Products	
NH_3 Ammonia (17)	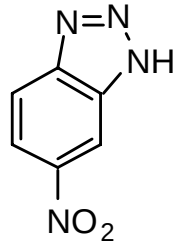 6 nitro-1,2,3 benzo triazole (164) (NBT)
H_2O Water (18)	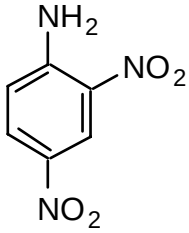 2,4 dinitro aniline (183) (DNA)
N_2 Nitrogen (28)	
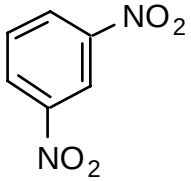 m-dinitrobenzene (DNB)	

Autocatalysis

The fact that NBT and DNA are observed prior to the evolution of the main decomposition products (DNB, NH_3, H_2O and N_2) suggests that the decomposition of DNPH may be controlled by an "autocatalytic-type" of process. This type of behavior has been observed in the decomposition of nitro compounds used as propellants and explosives. In these cases reactions that occur during the early stages of an experiment lead to the formation of a non-volatile residue, which has been found to play a major role in controlling the rate of decomposition during the later stages of the experiments. The early appearance of NBT and DNA along with its persistence after the DNPH is gone (green line in Fig. 5), suggests that this behavior may also be important in the decomposition of DNPH.

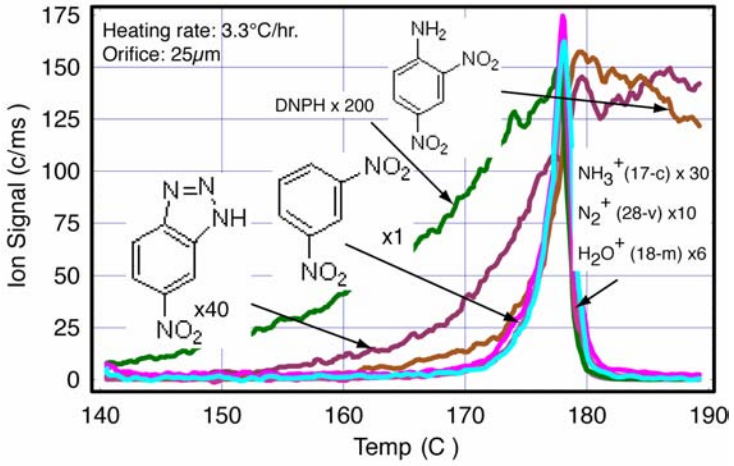

Figure 5. Temporal behavior of the ion signals associated with the compounds that evolve from the reaction cell as DNPH is heated and decomposes (DNPH016).

The “autocatalytic-type” of reaction process was investigated by running a set of experiments at 165°C under isothermal conditions. Examining the rate of evolution of decomposition products under isothermal conditions provides a simple means to determine if the accelerating rate of reaction associated with “autocatalytic-type” reactions is present.

In the first experiment (DNPH023) 6.64 mg of DNPH was decomposed in a reaction cell fitted with a 22 µm diameter orifice. The results are shown in Fig. 6A&B. In this experiment the ion signal associated with the evolution of DNPH (198) remains constant once the sample reaches the isothermal temperature and decreases as DNPH is depleted. After the sample reaches isothermal conditions, the rate of formation of the products is very low and increases with time. The rate of evolution of the higher molecular weight products, NBT and DNA, increase along with DNB and the low molecular weight products, NH_3, H_2O and N_2. However, careful examination shows that NBT and DNA continue to evolve after DNPH, DNB and the other lower molecular weight products are gone. This suggests that a relatively non-volatile compound is formed during the decomposition process and this compound may open new reaction pathways that control the decomposition of DNPH. This concept is consistent with the temporal behavior of the products that evolve during the reaction and also consistent with the formation of a black residue in the reaction cell at the end of the experiment. Since this black residue is of unknown composition, we refer to it as non-volatile residue (NVR). Thus, from these results one of the rate controlling reactions in the decomposition of DNPH is the interaction of DNPH with the NVR to form several volatile products and increase the amount of NVR. As the amount of NVR increases the reaction rate will increase.

To test this hypothesis, the black NVR formed in Experiment DNPH023 was left in the reaction cell

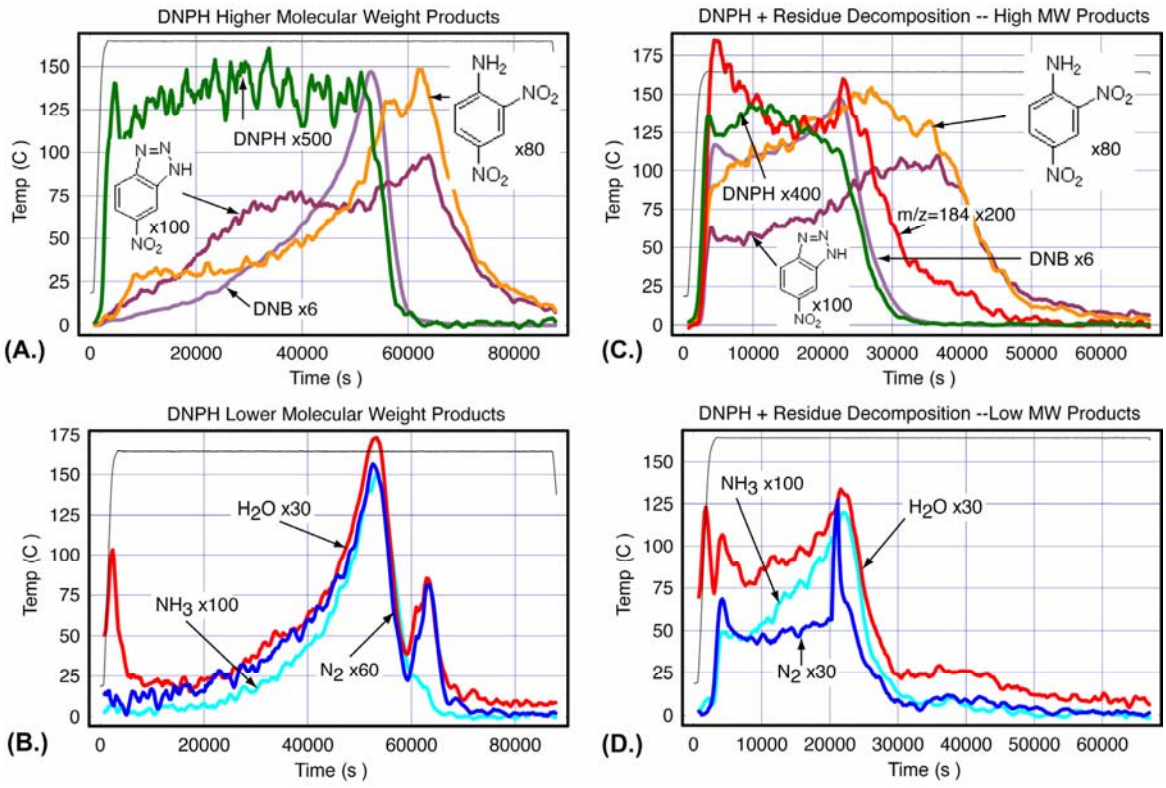

Figure 6. Ion signals representing the compounds that evolve during the decomposition of DNPH. Results from two experiments are presented DNPH023(A & B) and DNPH025 (C & D). Thin black line shows the temperature of the sample. Ion signals are in units of counts/ms.

and more DNPH was added. Using this mixture, another isothermal experiment was run at 165°C. The results are shown in Fig. 6 C&D. As can be seen from the results, the rates of evolution of the decomposition products are much higher as the sample reaches 165°C when the NVR is present at the start of the experiment. For example, the ion signal tracking the DNB product has a value of ~19 (110/6) in the experiment with the NVR, whereas it has a value of ~0.5 (3/6) at the same point in the experiment without the NVR (Fig. 6C vs. 6A). This result shows that reaction of DNPH with the NVR plays a major role in controlling the decomposition of DNPH. As in the first experiment, NBT and DNA continue to evolve from the sample after the DNPH is depleted, providing additional evidence that these two compounds originate from the NVR.

Rapid Heating/DSC Comparison

Differential scanning calorimetry (DSC) is often used to examine the heat evolved during the decomposition of energetic materials. In a typical DSC experiment the samples are heated more rapidly (0.5 to 10°C/min) than the samples in the experiments that have just been described (0.055 °C/min). To compare our slow heating result with those usually obtained in a DSC experiment, an experiment was conducted in which the sample was heated at 2°C/min (DNPH002). The results are shown in Fig. 7.

Comparison of the results from the slower heating rate experiments, Figures 5 and 6, with the results from the faster heating rate experiment shows that the products formed in the reaction are similar, but the temporal behavior of the evolution of the products are different. In the faster heating rate experiments, the major decomposition products, DNB, NH_3, H_2O and N_2, are first observed at ~200°C compared to 170°C for the slower heating rate experiments. Close inspection of the data in Fig. 7 also shows that the major decomposition products, DNB, NH_3, H_2O and N_2, evolve prior to the products associated with the decomposition of the NVR, NBT and DNA. This differs from the slower heating rate experiments in which the evolution of NBT and DNA were observed to precede the evolution of the major products.

Comparison of the results from the slower and faster heating rate experiments show that the faster

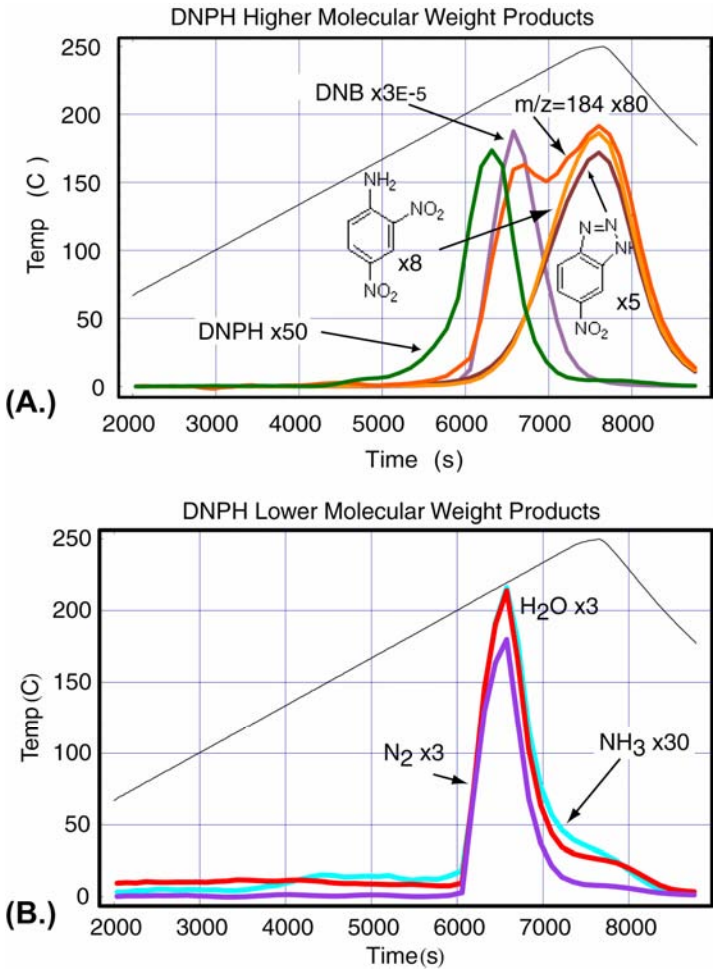

Figure 7. Ion signals representing the compounds that evolve during the decomposition of DNPH. Sample was heated at 2°C/min (DNPH002). Thin black line shows the temperature of the sample. Ion signals are in units of counts/ms.

heating rate experiments, which are characteristic of DSC experimental conditions, mask the true nature of the DNPH decomposition process. The "autocatalytic-like" nature of the decomposition process is not as obvious from the higher heating rate experiments, although they may be discerned from the temporal behavior of the various products. For DSC measurements, which measure heat evolution, the nature underlying process would not be apparent.

DNPH Summary

The decomposition of DNPH suggests that it is not, by itself, a good candidate to mitigate the violence of reaction in munitions. The products that evolve from the decomposition of DNPH are dominated by m-dinitrobenzene. Since the vapor pressure of DNB is relatively low and the amount of the more volatile products, NH_3, H_2O and N_2, is small, this suggests that DNPH will not, by itself, generate enough gas pressure to rupture the containment case of a munition.

Thus, for DNPH to serve as an ingredient that can mitigate the violence of reaction in a conventional munition, it must be able to interact with the other ingredients in the formulation to provide the required gas pressure. Next, we investigate the interaction of DNPH with RDX to determine whether or not DNPH will serve this purpose.

Decomposition of DNPH and RDX Mixtures

Mixtures of DNPH with RDX were examined to determine whether the mixtures of these two compounds would interact in a manner that would lead to a less violent reaction in a cookoff event. Again, the basic premise is that violence may be mitigated by rupturing the case of the munition prior to onset of rapid reaction of the energetic ingredients, such as RDX. It is also possible that violence of reaction may be mitigated by altering the properties of RDX that lead to its violent reaction. For example, converting RDX to another compound in a benign manner may also lead to less violent behavior.

In this phase of the project the interaction of DNPH and RDX was examined using the STMBMS instrument. Several experiments were also conducted using the FTICR mass spectrometer, in a manner described in the previous section, to identify the decomposition products formed by the interaction of DNPH with RDX. The experimental conditions for the series of experiments conducted on mixtures of RDX and DNPH are listed in Table A-III.

To obtain preliminary information on the interactions of DNPH with RDX, 1:1 mixtures of DNPH and RDX were examined. The DNPH was obtained from Arcos Chemical (sample DNPH01) and the RDX was a military grade material manufactured at Holston Defense Plant (Lot A-213). The 1:1 mixtures were chosen for initial experiments to provide the greatest interaction between the two materials. The initial experiments were conducted at isothermal temperatures (170°C to 190°C) in which we had previously observed the decomposition of RDX in the solid phase.[5] These experiments provided the first evidence of the interactions between DNPH and RDX and show that smaller amounts of DNPH in the presence of RDX would provide good experimental data and ratios of DNPH to RDX that were more likely to be used in a formulation. A ratio of 1:10 DNPH:RDX was selected for the subsequent experiments. In addition, the results from experiments with DNPH showed that slow heating rate experiments provide good insight into the reactions that control the decomposition of these compounds. Thus, the final set of experiment (and the ones presented here) are conducted with 1:10 mixture of DNPH/RDX and are examined at heating rates of 3.3°C/hour.

Ion Signals

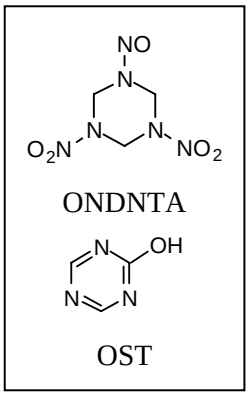

The identities of the products formed in the decomposition of mixtures of DNPH and RDX were determined from the high-resolution mass spectra of partially decomposed mixtures of the two ingredients. The m/z values, and formulas of each ion are listed in Table B-III.

The ion signals associated with the main compounds that evolve from the decomposition of Holston RDX as it is slowly heated at 3.3°C/hour are shown in Fig. 8. The ion signal associated with the evolution of RDX vapor from the reaction cell is shown in the upper panel. The ion signals associated with the main decomposition products are shown in the lower panel. Two higher molecular weight products are observed: 1-nitroso-3,5-dinitro-s-triazine (ONDNTA) and oxy-s-triazine (OST). Ion signals representing four of the lower molecular weight products are shown: CH_2O, NO, N_2O and NO_2. The ion signals representing these products first appear at ~165°C. The rates of formation of the products increase as the sample is heated. The data represents the behavior of the decomposition of RDX in the solid phase during the early stages of decomposition (first 25%). The main reaction products, CH_2O, N_2O and NO, are formed via the ONDNTA and NVR reaction pathways as described previously.[6-8] The minor amount of OST formed during decomposition suggests that the reactions occur in molten RDX on the surface of the RDX particles, since the direct reaction of RDX to form OST is primarily observed in the liquid phase.

The data on the decomposition of RDX presented in Fig. 8 serves as the baseline to which experiments examining the interaction of DNPH with RDX can be compared. Data from an experiment examining the decomposition of DNPH and RDX under similar conditions (DNPH022) are shown in Fig. 9.

The decomposition of mixtures of DNPH and RDX has features that are observed during the decomposition of individual ingredients as well as some features that are unique to the mixture. The data shown in Fig. 9 represents these various features. The ion signals that track the DNPH and RDX vapors are shown in the panel in Fig. 9A. The vapor pressure of both compounds increase as the sample is heated. The DNPH is gone at about 163°C as indicated by the ion signal from DNPH going to zero.

Effects on DNPH

The DNPH decomposes in a manner that is similar to that observed in experiments with only DNPH. The temporal behavior of this process is also similar to that observed with only DNPH, as indicated by the data in Fig. 9C. The main decomposition products from

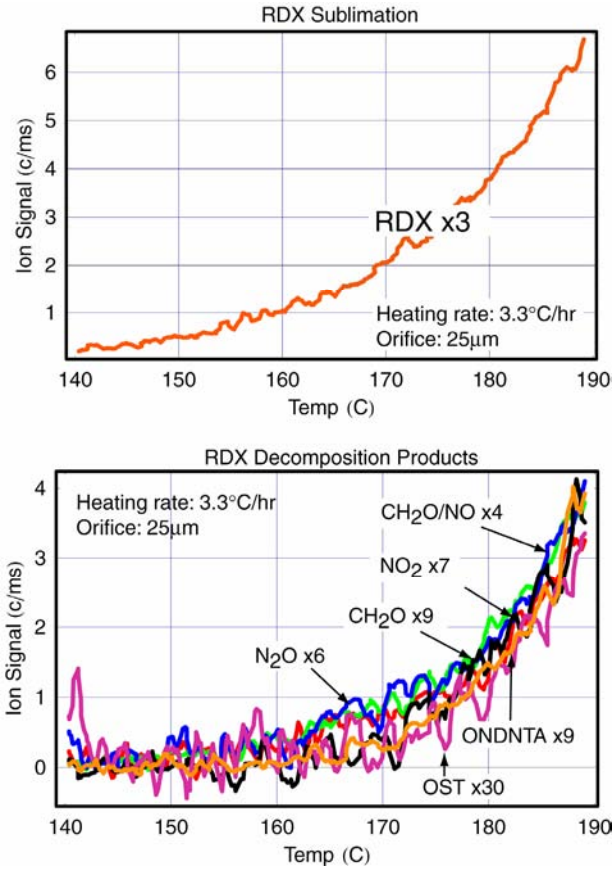

Figure 8. Ion signals associated with the main compounds that evolve during the decomposition of RDX (RDX297).

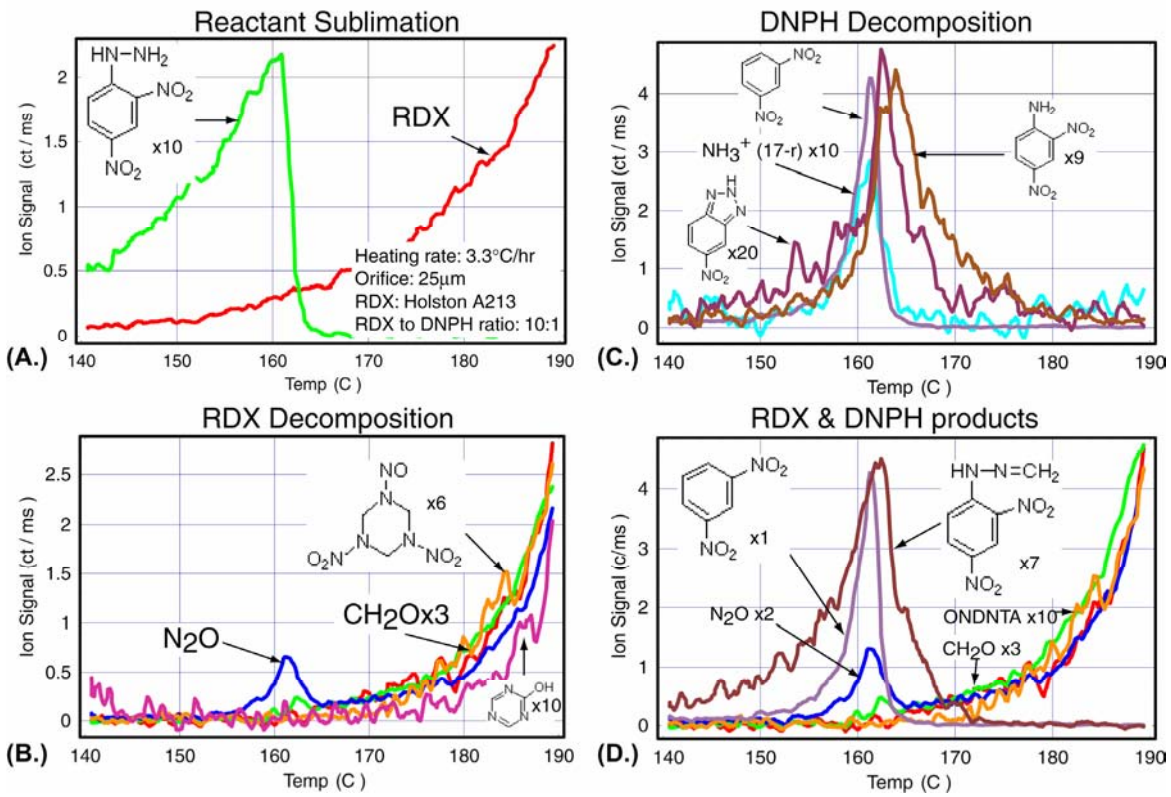

Figure 9. Ion signals associated with the main compounds that evolve during the decomposition of a mixture of DNPH and RDX using a 25µm diameter orifice (DNPH022).

DNPH are DNB, NH_3, H_2O and N_2. The two higher molecular weight products associated with the NVR that is formed in the decomposition of DNPH are also observed in the mixture: NBT and DNA. The main difference in the decomposition of DNPH in the mixture compared to its decomposition by itself is that decomposition in the mixture occurs at a lower temperature. The DNPH decomposes in a temperature range from 155°C to 163°C in the mixture, whereas by itself it decomposes in a temperature range from 172°C to 179°C (Fig. 5). This suggests that DNPH may either interact directly with RDX on the surface of the particles or the RDX may promote the formation of the NVR "autocatalyst" in the decomposition of DNPH, which results in DNPH decomposing at a lower temperature.

Effects on RDX

The decomposition of RDX in the mixture is similar to its decomposition by itself as indicated by the ion signals in Fig. 9B. The two higher molecular weight species formed during the decomposition are still ONDNTA and OST and the two lower molecular weight products are N_2O and CH_2O. The main difference between the decomposition of RDX in the mixture and by itself is the higher rate of formation of N_2O at about 161°C. Once the N_2O signal decreases, the behavior of the ion signals associated with the RDX decomposition products is similar to those observed in the decomposition of RDX by itself.

The higher rate of evolution of N_2O corresponds to the time interval in the experiment when DNPH is undergoing decomposition. A comparison of the ion signals associated with the compounds that can interact during the decomposition of DNPH and RDX are shown in Fig. 9D. Comparison of the N_2O,

CH_2O, DNB and DNPH signals illustrate the interaction between the ingredients. The N_2O signal appears to rise and fall in conjunction with the DNB signal. This suggests that the DNB may dissolve some of the RDX on the surface of the particles, leading to a higher rate of decomposition of the RDX that has been shifted from the crystalline phase into the solution with DNB. During the decomposition of RDX in the solid phase, N_2O and CH_2O are formed at comparable rates. Examination of the data in Fig. 9D shows that the signal from CH_2O remains near zero while the N_2O signal rises. This behavior is due to the well-known reaction between DNPH and aldehydes or ketones: DNPH reacting with CH_2O to form 2-methylene-1-(2,4-dinitrophenyl)hydrazine (m/z=210). The ion signal of the product of this reaction is shown in Figure 9D.

The results show that there is a reaction between DNPH and RDX, but reaction of the mixture does not lead to a large change in the decomposition behavior of either ingredient.

Changing Confinement

To determine whether confining the products formed in the decomposition of DNPH and RDX would enhance their rate of reaction, experiments similar to those shown in Fig. 9 were conducted using smaller orifices on the reaction cell (10 µm and 3 µm). The results from the decomposition of a mixture of DNPH and RDX using a 10µm and 3µm diameter orifices on the reaction cell are shown in Figures 10 and 11, respectively. The results from the two experiments using smaller diameter orifices in the reaction cell are qualitatively similar to the results from the experiment using the 25 µm diameter orifice (DNPH022). For the experiment using the 10µm diameter orifice, the main difference is that the temperature range over which the DNPH decomposes is about 4°C lower than that observed for the 25µm orifice. This is also true for the experiment using the 3µm orifice (Fig. 11). The experiment with the 3µm orifice shows several other differences. First, the signals from RDX and DNPH are very small (not plotted). This is due to the reduced flow rate of these compounds with the smaller diameter orifice. (Compounds present in more than one phase will maintain a constant vapor pressure at a given temperature.) This lower flow rate of multiphase

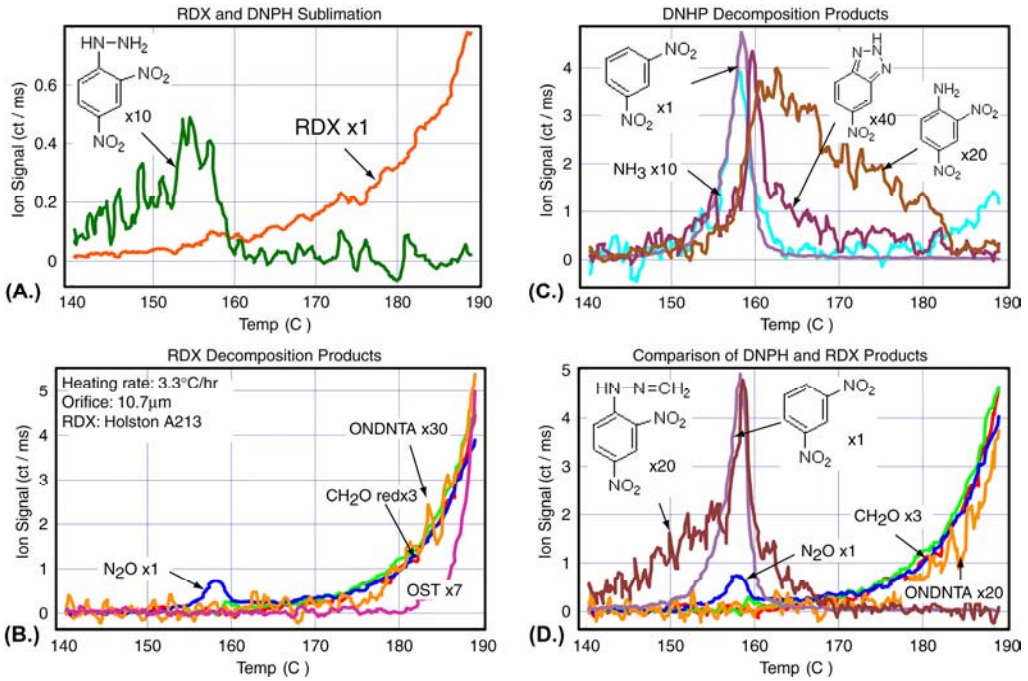

Figure 10. Ion signals associated with the main compounds that evolve during the decomposition of a mixture of DNPH and RDX using a 10µm diameter orifice (DNPH026).

compounds from the reaction cell is also apparent in the temporal behavior of DNB. Note that the DNB takes a longer period of time to evolve in this experiment. It is also interesting to note that the increased rate of N_2O formation from the decomposition of RDX also tracks the presence of DNB. This again suggests that interaction of DNB with RDX may account for the increased rate of RDX decomposition.

DNPH and IRDX Mixtures

The experiments presented so far have used standard Holston grade RDX. The interaction of DNPH with samples of RS-RDX was also investigated. The interaction of DNPH with SNPE and Dyno Noble RS-RDX are shown in Figures 12 and 13, respectively. The experiments were conducted using a reaction cell fitted with a 25µm orifice. The results may be compared to the interactions of DNPH with Holston grade RDX shown in Fig. 9. The basic features of the decomposition of each ingredient and the interactions between the ingredients are similar for each type of RDX. The main difference is that the temperature at which the DNPH reacts to form DNB is slightly different in each experiment. The DNB is observed at the lowest temperature in reactions with Holston RDX (peak at 160°C), it is observed at the highest temperature in reactions with SNPE RDX (peak at 164°C) and occurs at an intermediate temperature in interactions with Dyno Nobel RDX (peak at 162°C). Given that the

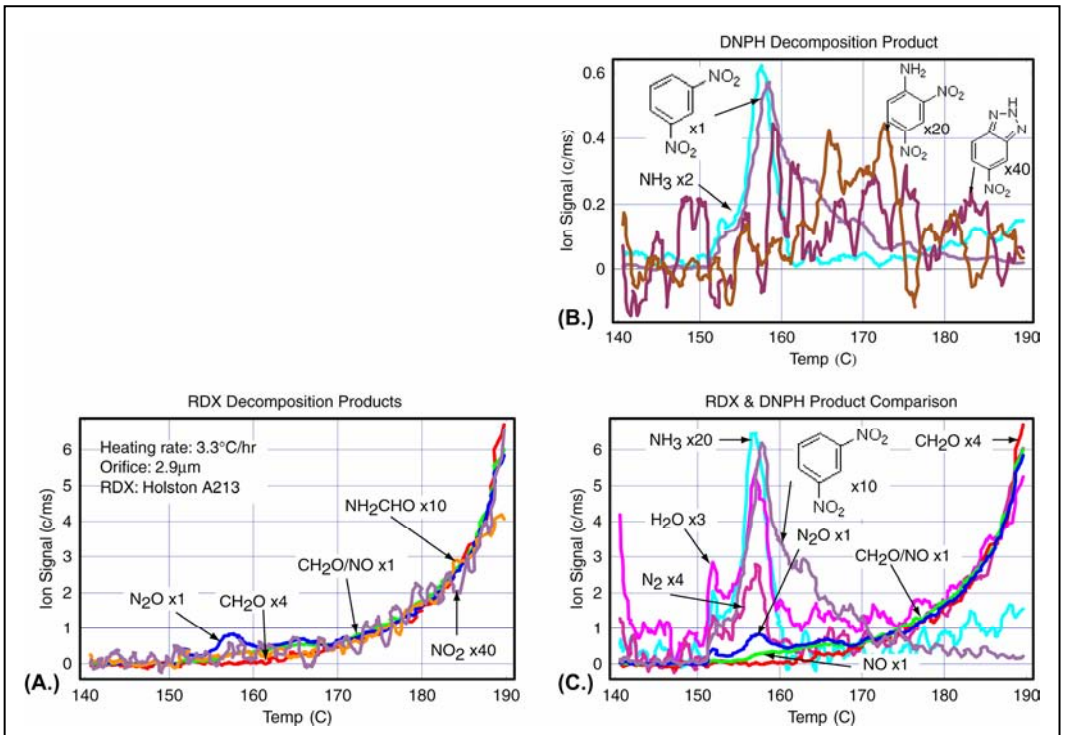

Figure 11. Ion signals associated with the main compounds that evolve during the decomposition of a mixture of DNPH and RDX using a 3µm diameter orifice (DNPH028).

purity of SNPE RDX is higher than the other two materials, the results suggest that the impurities in RDX may somehow interact with the DNPH decomposition process, resulting in increased reaction rates and evolution of the decomposition products at lower temperatures.

In summary, the decomposition of mixtures of DNPH and RDX are for the most part controlled by the decomposition processes of the individual ingredients. There is some limited interaction between the two ingredients. The main interaction results in the more rapid decomposition of RDX to N_2O and CH_2O during the period when DNPH decomposes. The increased rate of formation of N_2O

during this period is correlated with the formation of m-dinitrobenzene (DNB) formed in the decomposition of DNPH. The increased rate of RDX decomposition may result from RDX dissolving in the DNB where its reaction rate is likely to be higher than in the solid RDX powder. The other interaction observed is the reaction of DNPH with CH_2O to form 2-methylene-1-(2,4-dinitrophenyl)hydrazine (m/z=210).

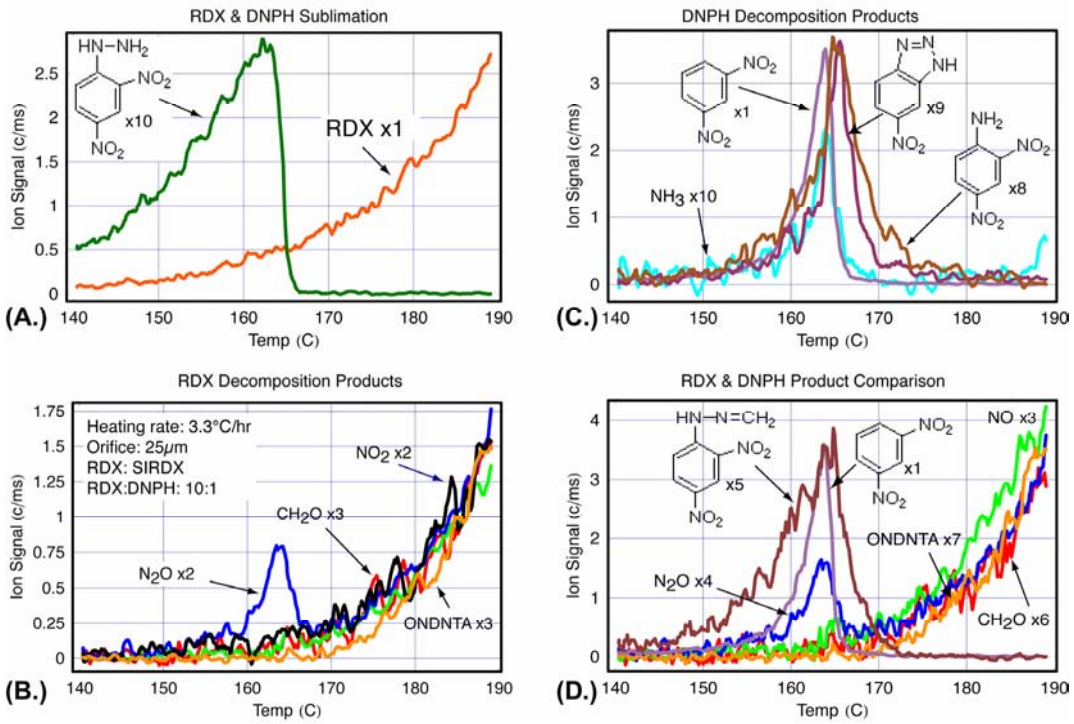

Figure 12. Ion signals associated with the main compounds that evolve during the decomposition of a mixture of DNPH and SNPE RS-RDX (DNPH032).

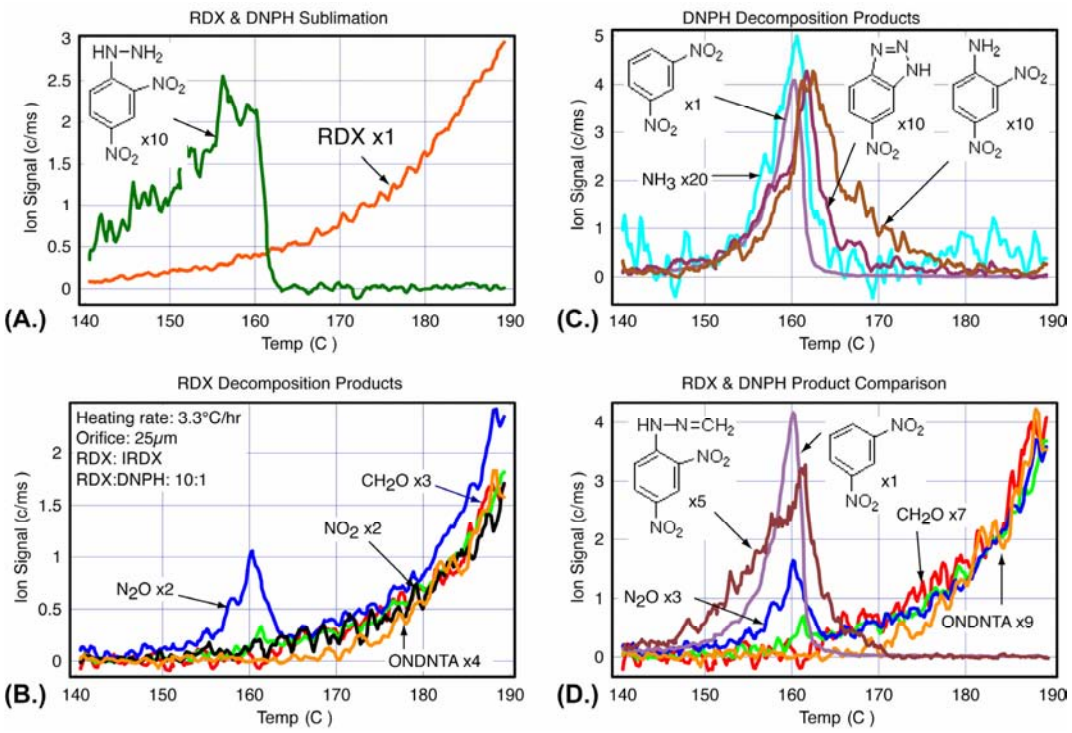

Figure 13. Ion signals associated with the main compounds that evolve during the decomposition of a mixture of DNPH and Dyno Nobel RS-RDX (DNPH034).

Insensitive RDX

Insensitive RDX.

Research to develop less shock sensitive RDX has focused on two features of the manufacturing process. First, high purity RDX, without HMX present in the sample, has been used to create the powders. Second, new crystallization methods have been developed to reduce the number of voids and other inclusions within the RDX particles. Experiments have shown that RDX particles with fewer inclusions have lower shock sensitivity.[9] Thus, reduced shock sensitivity of RDX is thought to be associated with the number of defects within the RDX crystal. Our results suggest that insensitive RDX powders may have other properties that may reduce the shock sensitivity of these materials.

While the main goal of this project was to investigate decomposition of DNPH and its interaction with RDX, a number of experiments have been conducted to investigate the properties of insensitive RDX. Four types of RDX have been examined (Table I). One sample is RDX manufactured at Holston Defense Plant sometime prior to 1985(RDX_01). The other three samples are insensitive RDX manufactured by SME Groupe SNPE and Dyno Nobel ASA. One of the RS-RDX samples made at SNPE uses RDX synthesized at Holston as the starting material for making the powder (IRDX_01). The other two powders are made using very high purity RDX as the starting material (IRDX_02 and IRDX_03).

The objective of the current study with regard to insensitive RDX is to ascertain whether or not the STMBMS apparatus can be used to identify differences between the properties of insensitive RDX, pure RDX and normal RDX that contains between 5% and 10% of HMX. To make this determination the STMBMS has been used to (1) examine the samples for contaminants, (2) measure the sublimation rates of the different RDX samples at low temperatures (50° to 100°C) and (3) to examine the decomposition of RDX in the solid phase below its melting point.

The results have shown significant differences between the four materials.

RDX vapor pressure results.

The vapor pressure of the four RDX samples have been measured by heating a sample of each material in a reaction cell fitted with a 1000µm diameter orifice. An example of the data collected in one of these experiments is shown in Figure 14. The sample is heated in a series of steps to a temperature of 100° and then is cooled in a series of steps. While the sample is heated the mass loss is measured with the microbalance and the ion signals from the evolving gas are measured with the mass spectrometer. The ion signal at m/z=128 is formed from RDX evolving from the reaction cell. The ion signal is combined with the data from the microbalance to

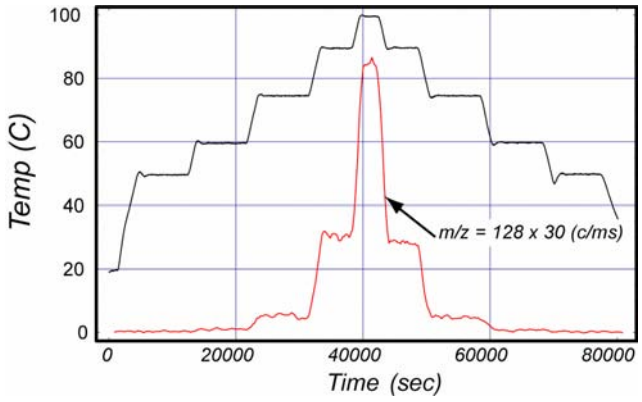

Figure 14. Example of data from experiment to measure RDX vapor pressure (RDX288). Ion signal at m/z=128 originates from RDX.

calculate the vapor pressure of RDX at each temperature step. For a pure compound the vapor pressure should be independent of the heating cycle and should not vary during the course of an experiment.

Vapor pressure data from the four different types of RDX powder are shown in Fig. 15. The data for all four materials were collected using a 1000 µm orifice under identical conditions, so that differences in behavior can be easily observed. (Note that the actual vapor pressure of RDX will be somewhat higher than shown in Fig. 15, since the large diameter orifice does not allow equilibrium to be established between sublimation and condensation on the surface of the RDX powder.) The data for the SNPE SIRDX powder (RDX288) and the Dyno-Nobel IRDX powder (RDX292) show that the vapor pressure (and thus the corresponding rate of sublimation) of RDX is higher when measured in the set of isothermal steps leading to 100°C than it is on the subsequent series of steps as the sample is cooled. This behavior differs from that observed in the vapor pressure experiments with Holston RDX. The results with both the powder manufactured by Holston (Holston (1985), RDX282) and the Holston RDX powder that was reprocessed by SNPE (RDX294) are shown in Fig. 15. In these two experiments the vapor pressure of the RDX prior to and after heating to 100°C are approximately the same.

The results from these four initial experiments investigating the sublimation characteristics of RDX are listed in Table III. The two insensitive RDX powders made by SNPE and Dyno-Nobel, using pure RDX have larger difference in their heats of sublimation prior to and after heating the sample to

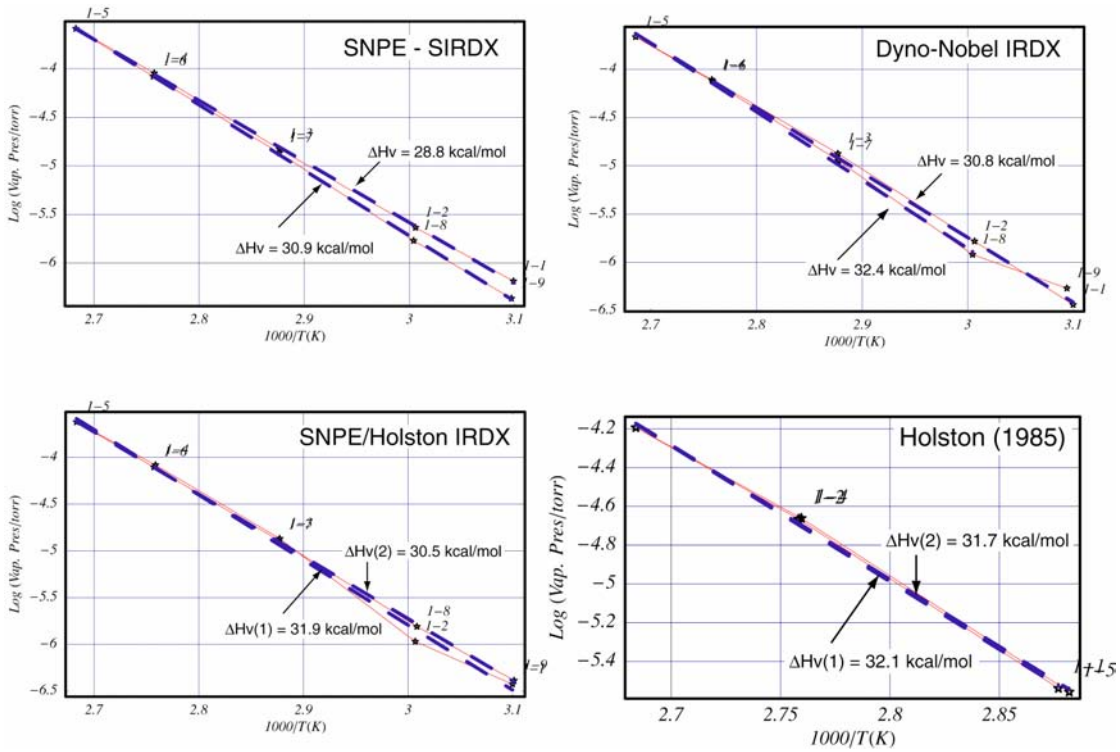

Figure 15. The vapor pressures of four different types of RDX powders are shown as they were heated in steps between 50°C and 100°C. The numbers by each data point indicate when the measurement was made during the experimental sequence. For the three insensitive RDX powders the vapor pressure was higher before the sample was heated to 100°C than after. The heats of sublimation for the sample before and after heating to 100°C are shown on each graph.

100°C. The table also lists the amount of the original sample (m) and the amount of material that evolved from the sample as it was heated to 100°C (Δm).

Table III. Vapor pressure data for different types of RDX powder.

Sample	*Manufacturer*	*Material*	*Experiment #*	*Δm/m**	*ΔHs (prior)*	*ΔHs (after)*
RDX_01	Holston	Holston	RDX282	0.17/4.72	32.1	31.7
IRDX_01	SNPE	Holston	RDX294	0.80/4.72	31.9	30.5
IRDX_02	SNPE	SNPE	RDX288	0.7/5.3	28.8	30.9
IRDX_03	Dyno-Nobel	Dyno-Nobel	RDX291	0.7/5.2	30.8	32.4

* Δm = weight loss on heating to 100°C, m = total starting weight of sample in mg

RDX decomposition results.

Thermal decomposition experiments using the different RDX powders were conducted to determine whether or not the type of RDX powder affected the decomposition processes. The experiments were conducted by heating the samples in a reaction cell with a 10 μm orifice and holding them at an isothermal temperature of 180°C. Previous experiments under these conditions had shown that at temperatures below the melting point RDX decomposes in a process that appears to occur on the surface of the particles.[5] The experimental conditions for each experiment are listed in Table IV. The ion signals associated with the two main decomposition products, CH_2O (m/z=30) and N_2O (m/z=44) are shown in Fig. 16.

Significant differences have been observed between the temporal behaviors of the gas evolution rates

Table IV. Experimental conditions for RDX decomposition experiments.

Sample	*Manufacturer*	*Material*	*Experiment #*	*Orifice Dia. (μm)*	*Δm/m* @time*
RDX_01	Holston	Holston	RDX278	5	na
IRDX_01	SNPE	Holston	RDX286	10.9	na
IRDX_02	SNPE	SNPE	RDX289	10.7	0.6/5.5 (18000)
IRDX_03	Dyno-Nobel	Dyno-Nobel	RDX292	10.6	0.6/5.0 (30000)

* Δm = weight loss on heating to 100°C, m = total starting weight of sample in mg.

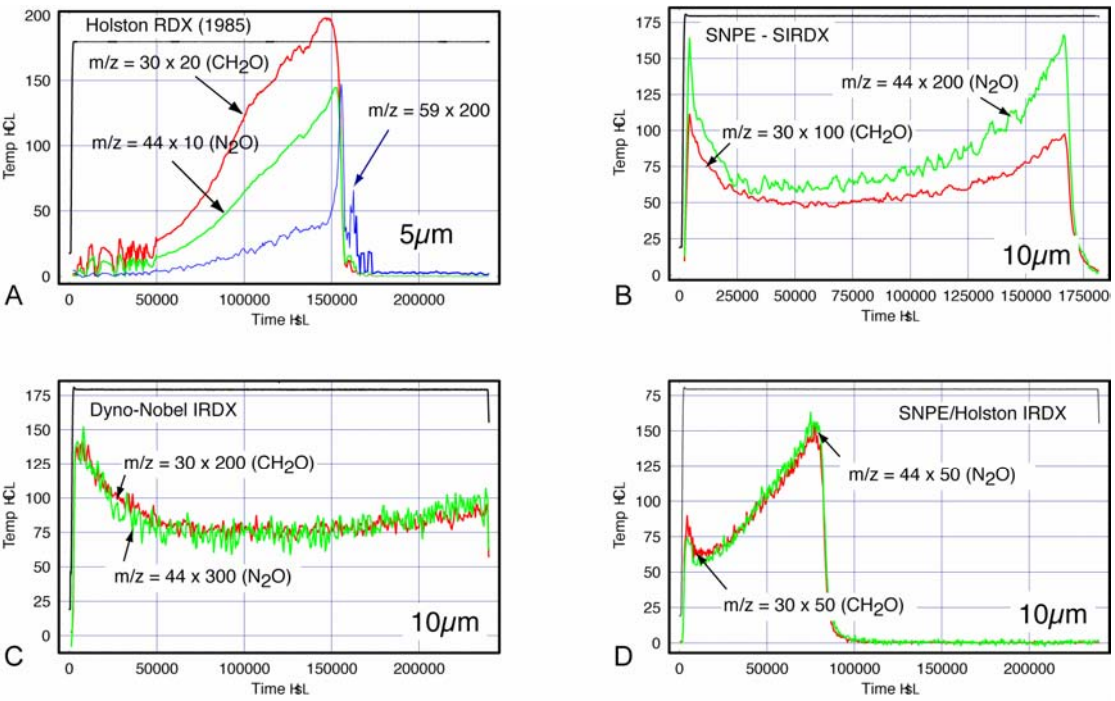

Figure 16. Ion signals representing two of the main decomposition products, CH_2O (30) and N_2O (44), formed during the decomposition of four different types of RDX powder.

of the two main decomposition products as the samples decomposed. The decomposition behavior of RDX from a typical lot of material from Holston is shown in Fig. 16A. In this experiment the initial rate of formation of CH_2O and N_2O are low. Their rates of formation increase with time as the nonvolatile products accumulate on the surface of the powders, leading to higher rates of reaction. The rates of formation of decomposition products in this experiment are higher than in the other three due to the smaller diameter orifice used in these experiments.

Ion signals from products formed in the decomposition of RS-RDX, manufactured by SNPE, are shown in Fig. 16B. The temporal behavior of the rates of formation of CH_2O and N_2O are different from the results with the Holston RDX. In this case the rates of formation of CH_2O and N_2O increase to a relatively high value when the sample first attains the isothermal temperature of 180°C. After a period of time, the rate of reaction slows and the rate of evolution of the reaction products decreases, settling to a constant value at ~25,000 seconds. After remaining roughly constant for a period of time, the rates of formation of CH_2O and N_2O increase in an autocatalytic-like manner, which is similar to the behavior observed for Holston RDX (Fig. 16A).

Ion signals from products formed in the decomposition of insensitive RDX, manufactured by Dyno-Nobel, are shown in Fig. 16C. The temporal behavior of the rates of formation of CH_2O and N_2O in this material is similar to that observed in the SNPE insensitive RDX (Fig. 16B). Again, the rates of formation of these two decomposition products achieve a maximum value when the sample first reaches 180°C and then decrease and settle at a relatively constant value after approximately 50000 seconds. Comparison of the relative intensities of the ion signals between the experiments with SNPE RDX and Dyno-Nobel RDX indicate the rate of formation of the decomposition products from the Dyno-Nobel material is slower. This lower signal intensity is also consistent with a slower rate of growth in the rate of formation of CH_2O and N_2O as the experiment progresses, indicating that the rate of the autocatalytic-like reaction is slower in the Dyno-Nobel RDX.

The temporal behavior of the rates of formation of CH_2O and N_2O in the decomposition of SNPE and Dyno-Nobel RDX is analogous to the temporal behavior of decomposition products formed in experiments with 2,4-dinitroimidazole (24DNI).[10, 11] In experiments with 24DNI it was shown that water was absorbed in the surface layers of the 24DNI particles, forming a shell-like structure around the particle in which the 24DNI was mixed with water. When the 24DNI decomposed in this shell-like structure the reaction rate of 24DNI was higher than in the internal core of the particle. This resulted in a higher rate of reaction when the 24DNI sample first reached its isothermal decomposition temperature and then decreased as the material in the shell-like structure was consumed in the decomposition process, creating ion signal from the decomposition products with temporal features that are the same as those observed in the decomposition of the SNPE and Dyno-Nobel insensitive RDX.

The increased rate of decomposition of SNPE and Dyno-Nobel insensitive RDX when they first reach the isothermal decomposition temperature suggests that the particles that constitute these powders may have an outer shell-like structure that differs from the core of the particles, as illustrated in the cutaway drawing of a particle. The RDX in the shell of these particles decomposes more readily, as indicated by the results of our decomposition experiments, and also sublimes more easily as indicated by our vapor pressure measurements.

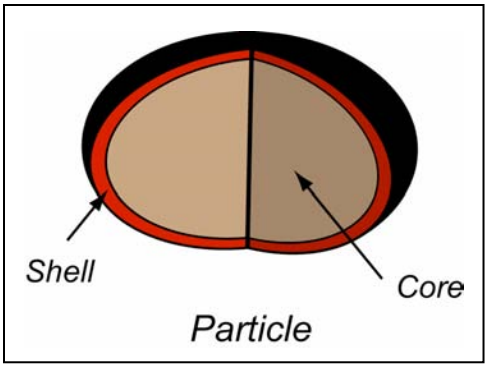

The thickness of the shell may be estimated from the amount of mass the sample has lost when the transition in the vapor pressure data or decomposition data is observed. The mass loss associated with the change in vapor pressure is listed in Table III and the mass loss associated with the more rapid decomposition is listed in Table IV. In both types of experiments the transition occurs when approximately 0.6 mg have been lost from a sample with an initial mass of ~ 5mg. Thus, assuming spherical particles, the ratio of the radius of the initial particle to the radius of the particle at the transition point is 0.96. Using this ratio, the thickness of the shell on a 50µm diameter particle would be ~ 1µm.

The decomposition behavior of the Holston RDX that was recrystallized by SNPE (IRDX_01) differs from either the Holston material (Fig. 16A) or the insensitive RDX materials from SNPE and Dyno-Nobel (Fig. 16B&C). The ion signals representing the evolution of CH_2O and N_2O from the SNPE processed Holston RDX (Fig. 16D) are much larger than those for the two insensitive materials. For example, the ion signal representing N_2O is four to six times larger with the SNPE processed Holston RDX than in the insensitive RDX samples. The other interesting feature of the CH_2O and N_2O signals for the RDX_01 sample is that the reaction rates rise to a very high level when the sample first reaches the isothermal temperature. Note the large difference in the temporal behaviors of these signals in the Holston processed RDX (Fig. 16A) and the SNPE processed RDX (Fig. 16D). In the Holston processed material the ion signals are very low when the sample first reaches the isothermal temperature. In the SNPE processes material the ion signals are much higher.

The high initial rate of formation of the decomposition products in the SNPE processed Holston RDX is reminiscent of experiments in which the role of the nonvolatile residue formed in the decomposition was examined.[8] In these experiments, NVR formed in one experiment was incorporated with RDX in a subsequent experiment to assess the reactivity of RDX with the NVR. It was found that if NVR is mixed with RDX the reaction rate of the RDX is much higher than observed in experiments with only RDX. These experiments showed that reaction of RDX with the NVR is the primary decomposition pathway of RDX in the solid phase. The temporal behavior of the evolution rates of CH_2O and N_2O in the experiments with mixtures of NVR and RDX is similar to the decomposition of the SNPE processed Holston RDX shown in Fig. 16D.

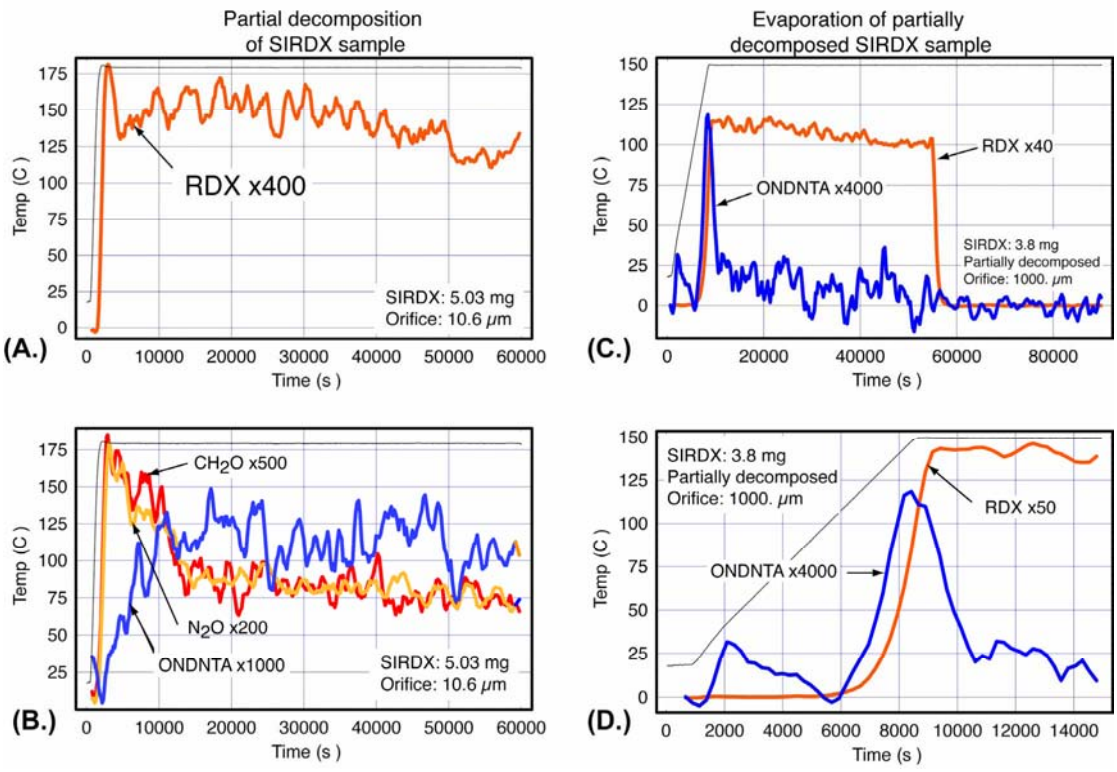

Figure 17. A& B) Ion signals from compounds that evolve from the reaction cell during the partial decomposition of an SNPE insensitive RDX sample (RDX302A). C&D) Ion signals from the compounds that evolve from the remaining RDX sample as it is sublimed in the STMBMS instrument.

The decomposition behavior of SNPE processed Holston RDX suggests that the processing procedure creates a powder that either contains some form of catalyst or can rapidly decompose to form the catalyst. The catalyst opens the more rapid reaction channel that involves formation of the NVR.

The data collected on the insensitive forms of RDX under this project are limited to the data presented in Figures 15 and 16. Additional data must be collected to verify these findings. In the future, additional experiments examining the vapor pressure will focus on collecting data with better signal to noise levels, providing more accurate data at lower temperatures. The data from the decomposition experiments show that the reactive processes that control the thermal decomposition of RDX below its melting point can be very dependent on subtle properties of the particles, which may be introduced during the manufacturing process. The results clearly indicate that the decomposition behavior of different types of RDX powders can vary widely under almost identical experimental conditions.

ONDNTA reaction pathway.

From the results of several of the experiments with RDX done under this project (Fig. 8), as well as experiments done previously with RDX, it is clear that the mononitroso analogue of RDX, ONDNTA, plays a major role in controlling its decomposition.[12, 13] To examine the role of ONDNTA in the decomposition of RDX in the solid phase, the decomposition of SNPE insensitive RDX was examined at 180°C. In this experiment, the sample was heated to 180°C and allowed to partially decompose (RDX302A). The experiment was stopped after ~25% mass loss. The reaction cell with the remaining sample was removed from the instrument, fitted with a larger diameter orifice (1000μm), returned to the instrument, and heated to an isothermal temperature of 150°C (RDX302B).

This allowed the remaining sample to vaporize and evolve from the reaction cell. The mass spectra of the vaporized material showed the presence of two compounds: RDX and ONDNTA. The ion signals from RDX, ONDNTA, CH_2O and N_2O formed during the decomposition experiment (RDX302A) are shown in Fig. 17A&B. The ion signals from the RDX and ONDNTA that evolve as the remaining sample is vaporized (RDX302B) are shown in Fig. 17C&D.

The data from the decomposition experiment (Fig. 17A&B) shows that the vapor pressure of RDX rises as the sample is heated and maintains a constant value in the reaction cell at the isothermal temperature(Fig. 17A). The ONDNTA signal takes about 10000 seconds to rise to a constant value. The fact that the ONDNTA signal does not rise to a steady-state value along with the RDX suggests that either some type of nucleation and growth process controls the creation of ONDNTA on the surface of the RDX particles or some feature of the RDX particle surface promotes the decomposition of the ONDNTA, not allowing ONDNTA to accumulate on the surface of the particles.

The results also show that the rate of evolution of CH_2O and N_2O is high while the rate of evolution of ONDNTA is low. Furthermore, the rates of evolution of CH_2O and N_2O decrease as the rate of evolution of ONDNTA increases. Thus, the temporal behavior of the rate of evolution of these three products during the early stages of decomposition suggests that there is some feature of the outer shell of the RDX particles that promotes the decomposition of ONDNTA to CH_2O and N_2O. It is interesting to note that the main products formed during the decomposition of ONDNTA are CH_2O and N_2O. The decomposition of ONDNTA is also known to form a large fraction of NVR.[13]

Eventually the rates of formation of CH_2O, N_2O and ONDNTA reach a steady state value at ~12000s. This suggests that at this point the rate of reaction of RDX to form ONDNTA and the rate of decomposition of ONDNTA to CH_2O and N_2O (as well as several other products not shown here) has reached a steady state condition. It also suggests that the ONDNTA is formed on the surface of the particles and not throughout the bulk of the RDX, since formation in the bulk would lead to an increasing rate of reaction.

The formation of ONDNTA on the surface of the RDX particles is consistent with the results from the vaporization experiment (Fig. 17C&D). The data shows that the composition of the vapor that evolves from the partially decomposed sample when it is first vaporized is enriched in ONDNTA. After a short period of time the rate of evolution of ONDNTA falls to zero and the remainder of the sample that evolves is composed solely of RDX. This demonstrates that ONDNTA is involved with reactions that occur on the surface of the RDX particles and does not form within the inner core of the RDX particles.

Previous studies on the decomposition of RDX in the liquid phase have shown that ONDNTA is formed by a reaction of RDX with NO.[6, 7] If this reaction controls the rate of formation of ONDNTA on the surface of the RDX particles, then confinement of the gaseous decomposition products would lead to higher pressures of NO in contact with the RDX powder. This, in turn, may increase the rate of diffusion of NO into the RDX and lead to a more rapid conversion of RDX to ONDNTA and its decomposition products. These products may react more slowly than RDX after the material ignites and lead to a less violent post-ignition explosion.

Discussion

Two unique experimental instruments have been used to probe the physical properties, and reactive processes involved in the thermal decomposition of energetic materials. The reaction processes have been examined over a range of temperatures that are important to understanding and characterizing the response of these materials in elevated thermal environments that are associated with abnormal thermal environments, such as those encountered in fires or malfunctions of artillery. The results from experiments conducted with these instruments have provided new understanding of how individual ingredients decompose and how ingredients in a mixture interact with each other. This understanding can be used to assess the behavior of existing explosive and propellant formulations. It can also be used to develop new materials that will enable the design of insensitive munitions. The STMBMS instrument has also been used to examine subtle differences in the physical properties and decomposition behavior of different forms of RDX, potentially providing new insight into why some forms of RDX may be less shock sensitive than others.

These instruments have been used to address the primary objective of this project: to assess whether a mixture of DNPH with RDX would provide a formulation that would mitigate the violence of reaction of explosive formulations containing RDX. The central premise of this concept to mitigate violence of reaction is to include an ingredient in the explosive formulation that would decompose prior to the energetic ingredients, generating a large quantity of gas, which would over pressurize the container, and rupture the case of the munition. The ingredient may generate a large quantity of gas either by its own decomposition or by its interaction with the energetic ingredients.

The experiments conducted in this project addressed several issues that underlie implementation of this mitigation concept. Two main issues were addressed: the decomposition of DNPH and its interaction with RDX.

First, the thermal decomposition of the additive, DNPH, was investigated. Several important questions were addressed: (1) What is its vapor pressure? (2) What are the decomposition products? (3) How rapidly does it decompose? (4) Will it generate gaseous decomposition products in sufficient quantity to rupture the case of the munition? (5) How mobile will it be in a formulation? (6) What are the contaminants? (7) How easy are they to remove? (8) Do contaminants affect the decomposition process? (9) Will they affect the long-term stability of the formulation?

Second, the interaction of DNPH with RDX was investigated. Several important questions concerning the mixture were addressed: (1) Does the decomposition of DNPH precede the decomposition of RDX? (2) Do the two ingredients interact during the decomposition process? (3) Will the decomposition process provide a significant amount of gas pressure that would rupture a munition case before the RDX ignites and explodes? (4) Is the RDX altered when it is heated in a manner that would lead to increased sensitivity? (5) Are there newly created defects that could function as hot spots? (6) How does confinement of the gases affect the reaction of the ingredients? (7) What effect will venting the gases have on the reaction of the ingredients and their ability to rupture the munition case? (8) Are the materials compatible?

Our findings on the decomposition of DNPH show that its vapor pressure is slightly less than that of RDX and its primary decomposition pathway produces 2,4-dinitrobenzene, H_2O, NH_3, and N_2. The vapor pressure of DNPH is high enough to make it sufficiently mobile to move through the gas phase to locations where it can interact with RDX or its decomposition products. Only two of the decomposition products will be useful for significantly increasing the pressure within a munition and rupturing the case: NH_3 and N_2. The partial pressure of the other decomposition products, 2,4-dinitrobenzene and water will be controlled by their two-phase equilibrium vapor pressure, which will not rise to a sufficiently high value to rupture most containment vessels. Thus, DNPH does not

appear to be a good candidate for mitigating the violence of reaction by its direct decomposition to form gaseous decomposition products that will lead to rupture of a containing vessel.

The more volatile decomposition products formed in the decomposition of DNPH originate from the hydrazine group. The remainder of the molecule, for the most part, is transformed to DNB. Two of the other larger molecules that are formed in the decomposition process, 2,4-dinitroaniline and 6-nitro-1,2,3 benzotriazole are both associated with a nonvolatile compound that is formed during the decomposition process. These products are observed both early in the decomposition process, before the DNPH has undergone substantial decomposition to DNB, H_2O, NH_3, and N_2, and late in the decomposition process, after the DNPH has completely decomposed. This behavior suggests that the nonvolatile residue is formed in the early stages of the decomposition process and may act as an autocatalyst in the reaction. This hypothesis was examined in a set of experiments in which the nonvolatile compound was collected and mixed with additional DNPH. The results from these experiments have shown that the nonvolatile compound does act as an autocatalyst in the decomposition process. Since DNPH does not appear to be a promising additive to mitigate reaction violence, the details of the autocatalytic reaction were not investigated further.

It is interesting to note that DNPH is another example of an organic material whose decomposition behavior in the condensed phase is controlled by a complex process in which nonvolatile products are formed in the early stages of decomposition and eventually come to control the overall behavior of the decomposition process. These complex processes involve coupled reaction pathways that open feedback pathways and introduce nonlinearities into the reaction system. The nonvolatile compounds often segregate into separate phases (i.e., a solid in the presence of a liquid or gas), which may have distinct morphological structures. In reactive systems such as these, processes that involve coupled spatial and temporal characteristics control the reactions. To understand such systems requires detailed experimental examination that is not typically possible using conventional thermal analysis methods such DSC. This difficulty has been illustrated in an STMBMS experiment conducted at a heating rate that is typical for DSC measurements (see Fig. 7). The results on the decomposition of DNPH illustrate how the STMBMS and FTICR mass spectrometric instrumental methods can be used to understand these complex reaction processes.

Our findings on the decomposition of mixtures of DNPH with RDX show that there is some limited interaction between these two compounds. The interaction does not significantly alter the decomposition behavior of either compound. The primary interaction is not through the direct interaction of DNPH with RDX, but rather through the interaction of decomposition products from each compound with the other reactant. Two primary interactions have been observed. In one reaction, DNB formed in the decomposition of DNPH interacts with the RDX leading to a faster rate of decomposition. This interaction is tracked by the increased rate of formation of N_2O from the decomposition of RDX. The increased rate of formation of N_2O coincides with the rapid decomposition of DNPH to form DNB. When the DNB is no longer present in the reaction cell, the rate of decomposition of RDX slows and assumes a reaction rate that is characteristic of RDX by itself. This behavior suggests that the DNB may dissolve some of the RDX on the surface of the RDX particles, leading to a more rapid decomposition of RDX that is in solution with DNB. Once the DNB is gone, the decomposition of RDX is again controlled solely by the reactions that occur in the RDX powder. In the second interaction, DNPH reacts with formaldehyde to form 2-methylene-1-(2,4-dinitrophenyl)hydrazine. This is a well-known reaction between DNPH and an aldehyde. (DNPH is a standard reagent used to detect aldehydes and ketones.) This reaction removes the CH_2O formed in the decomposition of RDX. The reaction takes place during the period when DNB is increasing the rate of decomposition of RDX. During this period of increased reaction rate of RDX, both N_2O and CH_2O should be observed at higher rates, since they are the main products of RDX decomposition in the condensed phase. What is observed is a higher rate of evolution of N_2O, but a near zero rate of evolution of CH_2O. At this stage the CH_2O is consumed in the reaction with DNPH.

Thus, about half of the gas that was formed in the increased rate of decomposition of RDX is consumed in the reaction with DNPH.

The decomposition of DNPH by itself or its interaction with RDX does not appear to generate a large amount of gaseous products. Thus DNPH does not appear to be a good candidate for an additive to mitigate the violence of reaction in cookoff scenarios. The amount of gas generated in its decomposition at cookoff temperatures is quite limited. Given the basic criteria for an additive to mitigate the violence of reaction, a material that will generate gas rapidly prior to onset of reaction in RDX is desired.

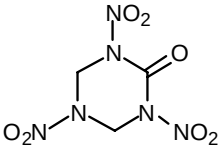

K-6

Several years ago we investigated the decomposition of a new energetic material, 2-oxo-1,3,5-trinitro-1,3,5triazacyclohexane (K-6). This compound is similar to RDX and its synthesis is relatively inexpensive.[14] The replacement of one of the methylene groups with a keto group results in K-6 decomposing in a simpler and more direct manner than RDX. The ion signals representing the products formed in the decomposition of K-6 are shown in Fig. 18. Two primary products are formed in the decomposition of K-6: CH_2O and N_2O. These two products are formed directly and rapidly from K-6. The decomposition starts between 150 and 155°C and is complete in our experiment by 180°C. This is below the temperature at which RDX starts to rapidly decompose. Thus, K-6 may be a good candidate to investigate as an additive for mitigating violence of reaction. It decomposes at a temperature below that of RDX and produces gaseous products (~ 6 moles of gas per mole of K-6) that will produce high pressures that are likely to rupture the case of a munition.

The recent development of new forms of RDX that have reduced shock sensitivity is of great interest for the development of less sensitive munitions. While card gap tests have shown these materials to be less sensitive, it is not understood how the properties of RS-RDX differ from conventional RDX. A number of studies[9] have shown that RS-RDX appears to have fewer solvent inclusions and defects contained within the RS-RDX particles compared to RDX produced at Holston. It has been suggested that the reduced number of defects within the insensitive RDX particles is responsible for its reduced shock sensitivity. It is also possible that eliminating the HMX from the RDX used to make the insensitive RDX powders may also be responsible for its reduced shock sensitivity. The lower melting point of Holston RDX powder (~185°C to 190°C) compared to pure RDX (~201°C) indicates that some portion of the HMX in the Holston RDX powders is included in the RDX particles, forming a solid solution of the two compounds.

In the limited number of experiments with insensitive RDX in this project, we have observed two features in which the properties of the insensitive RDX materials differ from the normal Holston RDX. In one feature we have observed that the vapor pressure of insensitive RDX is higher than Holston RDX when it is first heated. This suggests that RDX on the surface of the insensitive RDX particles may be less stable than RDX on the

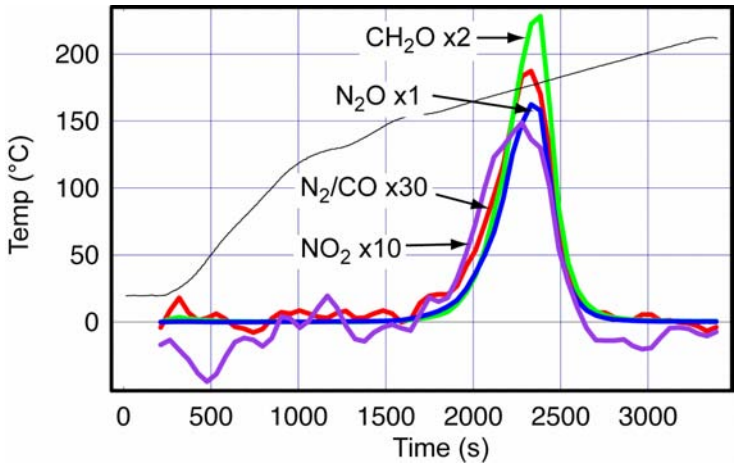

Figure. 18. Ion signals representing the main products formed in the decomposition of K6 as a function of temperature. Ion signals are in counts/ms.

surface of Holston RDX, making it easier for RDX to sublime from insensitive RDX particles. The second feature we have observed is that the rate of decomposition of RDX in the solid phase (at 180°C) is higher for a short period of time when the sample is first heated to the decomposition temperature. We have observed that during the initial period of decomposition, the rate of formation of CH_2O and N_2O are higher and the concentration of the ONDNTA reaction intermediate is lower. Eventually, the rates of formation of CH_2O and N_2O decrease to a steady level and the concentration of ONDNTA rises to a steady level. This steady rate of formation of the products occurs when the diameter of the particle has decreased by ~ 5%.

Both the higher sublimation and decomposition rates observed during the early stages of each type of experiment are consistent with the insensitive RDX particles having a shell-like structure on the outside of the particles. The results from our experiments suggest that the material in this shell-like structure is less stable than the RDX in the core of the particles. It is possible that RDX in the shell-like structure may be less well crystallized than the RDX in the core of the particles. It is also possible that some solvent or water may be incorporated in the shell-like structure, leading to more rapid decomposition.

This shell-like structure on the outside of the particles may be responsible for the decreased shock sensitivity. The same "hot-spot" arguments used to explain the reduced shock sensitivity due to fewer defects within the RDX particles can also be used to explain the effect of a less stable shell on the surface of the particles. The RDX particles slide past each other more easily. This may be similar to the reduction of sensitivity when powders of energetic materials are mixed with binders to form explosive or propellant formulations.

Further experiments need to be conducted to confirm the results of the initial experiments conducted in this project. In addition, other experiments and tests should be conducted in which the surface of the powders is altered and the shock sensitivity of the altered materials is compared to the shock sensitivity of the original RS-RDX materials. If these experiments demonstrate that the nature of the surface of the insensitive RDX particles plays a role in their decreased shock sensitivity, then further work can be undertaken to explore this property and possibly utilize this concept to develop less sensitive powders of other types of energetic compounds.

Conclusions

The STMBMS and FTICR mass spectrometry experimental methods have been successfully used to probe the decomposition of DNPH and its interaction with RDX to determine whether DNPH is a good candidate for an ingredient that can be used to mitigate the cookoff violence of conventional munition using RDX. It was found that the products formed in the decomposition of DNPH are dintrobenzene, ammonia, water and nitrogen. Of these compounds only nitrogen and ammonia are capable of generating high pressures within a munition and the amount of each formed in the decomposition of DNPH is relatively low. Thus, DNPH by itself is not a good candidate to mitigate the violence of reaction.

The interaction of DNPH with RDX is also limited. An increase in the rate of decomposition of RDX was observed when DNPH decomposed to form DNB. The DNB most likely dissolves some RDX from the surface of the particles, which leads to a higher rate of decomposition and increases the rate of formation of N_2O and CH_2O, its primary decomposition products. The overall increase in the rate of decomposition was limited. Furthermore, one of the gases, CH_2O, was removed from the system by reacting with DNPH to form a relatively nonvolatile product. Thus, the interaction of DNPH with RDX will not produce the large quantity of gas needed to rupture the case of a munition.

Better candidates for compounds that can be added to RDX-based formulations to mitigate violence of reaction should be capable of forming larger quantities of gaseous decomposition products below the onset of rapid reactions in HMX. One compound that may be a good candidate is a keto analogue of RDX, known as K-6.

Examination of several different forms of RDX has shown that the sublimation rates and decomposition behavior of RS-RDX differ from Holton grade RDX. The results suggest that the RS-RDX materials from both SNPE and Dyno-Nobel may have a shell-like structure of RDX on the surface of the particles that is less stable and more reactive than the material in the core of the particles. The origin of this shell-like RDX structure is uncertain, but may be due to some aspect of the manufacturing process. It is possible that this less stable RDX on the surface of the particles may be more fluid than the interior of the particles, allowing more slip between the surface of the particles under impact or shock. This may play a role in the reduced shock sensitivity of the insensitive RDX materials.

The experimental methods used in this study have provided new insight into the reaction of DNPH and RDX. While DNPH is not a good candidate for an additive to mitigate the violence of reaction, the experimental methods can be used in the future to investigate more promising candidates such as K-6. In addition, further examination of the behavior of insensitive RDX materials to determine if they have an outer shell of some modified form of RDX that reduces their shock sensitivity would be valuable for development of insensitive munitions.

Acknowledgements

This project has been undertaken in conjunction with Dr. Barry Fishburn (U.S. Army TACOM-ARDEC) and has been supported by the U.S. Army – Picatinny Arsenal under Work for Others Project #083030604a-00.

Bibliography

1. Fishburn, B.D., R.P. Ho, and S.K. Singh, *A Staged Explosive to Mitigate Cook Off Violence: Preliminary Work With 2,4-Dinitrophenyl Hydrazine*. 2003, U.S. Army, TACOM-ARDEC: Picatinny Arsenal.
2. Behrens, R., Jr., *New simultaneous thermogravimetry and modulated molecular beam mass spectrometry apparatus for quantitative thermal decomposition studies.* Review of Scientific Instruments, 1987. 58(3): p. 451-461.
3. Behrens, R., Jr., *Identification of Octahydro-1,3,5,7-tetranitro-1,3,5,7-tetrazocine (HMX) Pyrolysis Products by Simultaneous Thermogravimetric Modulated Beam Mass Spectrometry and Time-of-Flight Velocity-Spectra Measurements.* International Journal of Chemical Kinetics, 1990. 22: p. 135-157.
4. Behrens, R., Jr., *Determination of the Rates of Formation of Gaseous Products from the Pyrolysis of Octahydro-1,3,5,7-tetranitro-1,3,5,7-tetrazocine (HMX) by Simultaneous Thermogravimetric Modulated Beam Mass Spectrometry.* International Journal of Chemical Kinetics, 1990. 22: p. 159-173.

5. Maharrey, S., R. Behrens, and L. Johnston, *Physical and Chemical Processes Controlling the Solid-Phase Thermal Decomposition of hexahydro-1,3,5-trinitro-s-triazine (RDX)*, in *19th PSHS Mtg*. 2000, Chemical Propulsion Information Agency: Monterey, CA. p. 17 - 32.

6. Behrens, R. and S. Bulusu, *Thermal-Decomposition Of Energetic Materials .3. Temporal Behaviors Of the Rates Of Formation Of the Gaseous Pyrolysis Products From Condensed-Phase Decomposition Of 1,3,5-Trinitrohexahydro-S-Triazine.* Journal Of Physical Chemistry, 1992. 96(#22): p. 8877-8891.

7. Behrens, R. and S. Bulusu, *Thermal-Decomposition Of Energetic Materials .4. Deuterium-Isotope Effects and Isotopic Scrambling (H/D; C-13/O-18; N-14/N-15) In Condensed-Phase Decomposition Of 1,3,5-Trinitrohexahydro-S-Triazine.* Journal Of Physical Chemistry, 1992. 96(#22): p. 8891-8897.

8. Behrens, R. and S. Maharrey, *Chemical and Physical Processes that Control the Thermal Decomposition of RDX and HMX*, in *Combustion of Energetic Materials*, K.K. Kuo and L.T. DeLuca, Editors. 2002, Begell House: New York. p. 3 - 21.

9. Baillou, F., et al., *Influence of Crystal Defects on Sensitivity of Explosives*, in *Tenth International Detonation Symposium*, J.M. Short, Editor. 1993, Office of Naval Research, ONR 33395-12: Boston, Massachusetts. p. 816 - 823.

10. Minier, L., R. Behrens, and S. Bulusu. *Solid-Phase Decomposition of 2,4-Dinitroimidazole (2,4-DNI)*. in *Decomposition, Combustion and Detonation Chemistry of Energetic Materials*. 1996. Boston, MA: Material Research Society.

11. Behrens, R., L. Minier, and S. Bulusu, *Coupling Experimental Data and a Prototype Model to Probe the Physical and Chemical Processes of 2,4-Dintiroimidazole Solid-Phase Thermal Decomposition*, in *34th JANNAF Combustion Subcommittee Meeting*, CPIA, Editor. 1997, CPIA Publication # 662: West Palm Beach, FL. p. 549-567.

12. Behrens, R., Jr., T.A. Land, and S. Bulusu, *Thermal Decomposition Mechanisms of 1-Nitroso-3,5-dinitro-s-triazine (ONDNTA)*, in *30th JANNAF Combustion Meeting*. 1993, Chemical Propulsion Information Agency: Monterey, California. p. 47-59.

13. Behrens, R. and S. Bulusu, *The Importance of Mononitroso Analogues of Cyclic Nitramines to the Assessment and the Safety of HMX-Based Propellants and Explosives*, in *Challenges in Propellants and Combustion 100 Years after Nobel*, K.K. Kuo, Editor. 1997, Begell House, Inc.: New York. p. 275 - 289.

14. Mitchell, A.R., et al., *Synthesis, Scale-up, and Characterization of K-6*. 1991, Lawrence Livermore National Laboratory.

Appendix

Table. 2. Experiments with DNPH

Table A-I: Experiments with DNPH								
Experiment Name	**Experiment Type**	**Type of Heating**	**Heating Rate (s)**	**Maximum Temp. °C**	**Orifice Diameter**	**Sample Size (mg)**	**Material**	**Residue Weight (mg)**
DNPH001	Mass Spec	Simple Ramp	1C/min to 200C	200	977.9µm	11.83	DNPH01	4.37
DNPH003	Vapor Pressure	Ramp & Isothermal	2C/min to 60 1C/min steps; 70C to 140C by 10 isothermal	140	977.9µm	11.37	DNPH01	9.38
DNPH002	Decomposition	Simple Ramp	2C/min to 250C	250	19.86µm	9.2	DNPH01	5.07
DNPH004	Decomposition	Isothermal	4C/min to 170 1C/min to 180 0.5C/min to 190	190	21.61µm	6.02	DNPH01	1.39
DNPH006	Decomposition	Isothermal	8C/min to 160 4C/min to 170 1C/min to 175 0.5C/min to 180	180	7.82 µm	5.34	DNPH01	2.5
DNPH007	Vapor Pressure	Ramp & Isothermal	2C/min to 60 1C/min steps; 70C to 150C by 10 isothermal	150	977.9µm	3.4	DNPH01	0.05
DNPH013	Partial Decomp for FTICR analysis	Ramp	2C/min to 150C 0.5C/min to quench T.	179.5	20.32µm	2.25	DNPH01	2.11

Table A-I: Experiments with DNPH								
Experiment Name	**Experiment Type**	**Type of Heating**	**Heating Rate (s)**	**Maximum Temp. °C**	**Orifice Diameter**	**Sample Size (mg)**	**Material**	**Residue Weight (mg)**
DNPH015	Partial Decomp for FTICR analysis	Ramp	2C/min to 150C 0.5C/min to quench T.	191	19.5 µm	2.71	DNPH01	2.35
DNPH016	Decomposition	Slow Ramp	2C/min to 140 0.05C/min to 190	190	21.45µm	8.23	DNPH01	2.52
DNPH019	Mass Spec	Simple Ramp	1C/min to 200C	200	977.9µm	8.98	DNPH02	0.09
DNPH020	Decomposition	Isothermal	4C/min to 170 1C/min to 180 0.5C/min to 190	190	21.03µm	6.55	DNPH02	2.44
DNPH021	Decomposition	Isothermal	4C/min to 145 2C/min to 155 1C/min to 160 0.5C/min to 165	165	20.54 µm	5.46	DNPH01	5.03
DNPH023	Decomposition	Isothermal	4C/min to 145 2C/min to 155 1C/min to 160 0.5C/min to 165	165	22.18µm	6.64	DNPH02	2.25
DNPH025	Decomposition (Catalytic)	Isothermal	4C/min to 145 2C/min to 155 1C/min to 160 0.5C/min to 165	165	22.07µm	5.01 + residue	DNPH02	1.48

Table. 3. Experiments with RDX

Table A-II: Experiments with RDX								
Experiment Name	**Experiment Type**	**Type of Heating**	**Heating Rate (s)**	**Maximum Temp. ^{o}C**	**Orifice Diameter**	**Sample Size (mg)**	**Material**	**Residue Weight (mg)**
RDX282	Vapor Pressure	Ramp & Isothermal	1C/min to 50,60, 75,90 and 100 -1C/min to 90 75,60,50 then cool hold at each step.	100	978 µm	4.71	RDX-A213	4.56
RDX283	Decomposition	Isothermal	8C/min to 160 4C/min to 170 1C/min to 175 0.5c/min to 180	180	103 µm	3.86	RDX-A213	0.45
RDX286	Decomposition	Isothermal	10C/min to 150 4C/min to 170 2C/min to 175 1C/min to 180	180	10.9 µm	4.57	IRDX-01 HIRDX	0.31
RDX287	Mass Spec	Ramp	1C/min to 240C	240	978µm	4.69	IRDX-02 SIRDX	0.22
RDX288	Vapor Pressure	Ramp & Isothermal	1C/min to 50,60, 75,90 and 100 -1C/min to 90, 75,60,50 then cool hold at each step	100	973µm	4.71	IRDX-02 SIRDX	3.93
RDX289	Decomposition	Isothermal	10C/min to 150 4C/min to 170 2C/min to 175 1C/min to 180	180	10.7 µm	5.51	IRDX-02 SIRDX	0.03
RDX291	Vapor Pressure	Ramp & Isothermal	1C/min to 50,60,	100	973µm	5.31	IRDX-03	4.59

Table A-II: Experiments with RDX								
Experiment Name	**Experiment Type**	**Type of Heating**	**Heating Rate (s)**	**Maximum Temp. °C**	**Orifice Diameter**	**Sample Size (mg)**	**Material**	**Residue Weight (mg)**
			75,90 and 100 -1C/min to 90, 75,60,50 then cool hold at each step				IRDX	
RDX292	Decomposition	Isothermal	10C/min to 150 4C/min to 170 2C/min to 175 1C/min to 180	180	10.7 µm	4.96	IRDX-03 IRDX	0.85
RDX293	Mass Spec	Ramp	1C/min to 240C	240	978µm	4.90	IRDX-01 HIRDX	0.16
RDX294	Vapor Pressure	Ramp & Isothermal	1C/min to 50,60, 75,90 and 100 -1C/min to 90, 75,60,50 then cool hold at each step	100	973 µm	5.16	IRDX-01 HIRDX	4.43
RDX295	Mass Spec	Ramp	1C/min to 240C	240	978µm	5.35	RDX-A213	0.17
RDX297	Decomposition	Slow Ramp	2C/min to 140C 0.05C/min to 205C	205	22.0µm	4.73	RDX-A213	0.22
RDX301	Mass Spec	Ramp	1C/min to 240C	240	978µm	5.02	IRDX-03 IRDX	0.12
RDX302A	Partial Decomposition	Isothermal	10C/min to 150 4C/min to 170	180	10.6 µm	5.03	IRDX-02	3.79

Table A-II: Experiments with RDX								
Experiment Name	**Experiment Type**	**Type of Heating**	**Heating Rate (s)**	**Maximum Temp. °C**	**Orifice Diameter**	**Sample Size (mg)**	**Material**	**Residue Weight (mg)**
			2C/min to 175 1C/min to 180					
RDX302B	Evaporation	Isothermal	1C/min to 150C hold	150	96.5µm	3.79	IRDX-02 SIRDX	0.03
RDX305	Vapor Pressure	Ramp & Isothermal	1C/min to 50,60, 75,90 and 100 -1C/min to 90, 75,60,50 then cool hold at each step	100	978 µm	4.82	IRDX-02 **Aged SIRDX**	4.05
RDX306	Decomposition	Isothermal	10C/min to 150 4C/min to 170 2C/min to 175 1C/min to 180	180	11.1 µm	5.14	IRDX-02 **Aged SIRDX**	
RDX307	Decomposition	Isothermal	10C/min to 150 4C/min to 170 2C/min to 175 1C/min to 180	180	10.9 µm	5.11	IRDX-01 **Aged HIRDX**	0.47
RDX308	Decomposition	Isothermal	10C/min to 150 4C/min to 170 2C/min to 175 1C/min to 180	180	11.7 µm	5.40	IRDX-03 **Aged IRDX**	0.26
RDX309	Decomposition	Isothermal	10C/min to 150 4C/min to 170 2C/min to 175 1C/min to 180	180	11.8 µm	5.26	RDX-A213 **Aged A213**	0.53

Table. 4. Experiments with Mixtures of DNPH and RDX

Table A-III: Experiments with mixtures of RDX and DNPH

Experiment Name	Experiment Type	Type of Heating	Heating Rate (s)	Maximum Temp. °C	Orifice Diameter	Sample Size (mg)	Material	~ Residue Weight (mg)
DNPH005	Mass Spec 1:1 ratio	Simple Ramp	1C/min to 200	200	997.9µm	5.15 5.30	DNPH01 RDX-A213	0.13
DNPH008	Decomposition 1:1 ratio	Isothermal	8C/min to 160 4C/min to 170 1C/min to 175 0.5C/min to 180	180	11.23µm	4.93 5.07	DNPH01 RDX-A213	3.16
DNPH009	Decomposition 1:1 ratio	Isothermal	8C/min to 160 4C/min to 170 1C/min to 175 0.5C/min to 180	180	103.1µm	4.96 4.96	DNPH01 RDX-A213	1.49
DNPH010	Decomposition 1:1 ratio	Isothermal	8C/min to 160 4C/min to 170 1C/min to 175 0.5C/min to 180	180	104.8µm	5.28 5.32	DNPH01 RDX-A213	2.59
DNPH011	Decomposition 1:1 ratio	Isothermal	8C/min to 160 4C/min to 170 1C/min to 175 0.5C/min to 180	180	103.1µm	3.05 3.17	DNPH01 RDX-A213	0.85
DNPH012	Decomposition 1:1 ratio	Isothermal	8C/min to 150 4C/min to 160	170	96.5µm	2.99 3.06	DNPH01 RDX-A213	1.62

Table A-III: Experiments with mixtures of RDX and DNPH								
Experiment Name	**Experiment Type**	**Type of Heating**	**Heating Rate (s)**	**Maximum Temp. °C**	**Orifice Diameter**	**Sample Size (mg)**	**Material**	**~ Residue Weight (mg)**
			1C/min to 165 0.5C/min to 170					
DNPH014	Partial Decomp for FTICR analysis	Ramp	2C/min to 150C 0.5C/min to quench T	176.3	23.2µm	1.41 1.81	DNPH01 RDX-A213	2.66
DNPH017	Decomposition	Slow Ramp	2C/min to 140C 0.05C/min to 190C	190	21.85µm	3.64 3.63	DNPH01 RDX-A213	2.51
DNPH018	Decomposition 1: 6 ratio	Isothermal	8C/min to 160 4C/min to 170 1C/min to 175 0.5C/min to 180	180	103.1µm	0.75 4.54	DNPH01 RDX-A213	0.66
DNPH022	Decomposition 1:10 ratio	Slow Ramp	2C/min to 140C 0.05C/min to 190C	190	21.86µm	0.44 4.22	DNPH01 RDX-A213	2.44
DNPH024	Decomposition 1:2 ratio	Isothermal	4C/min to 145 2C/min to 155 1C/min to 160 0.5C/min to 165	165	23.18µm	1.99 3.99	DNPH02 RDX-A213	3.23
DNPH026	Decomposition 1:10 ratio	Slow Ramp	2C/min to 140C 0.05C/min to 190C	190	10.7 µm	0.46 4.23	DNPH01 RDX-A213	3.29
DNPH027	Decomposition 1:10 ratio	Slow Ramp	2C/min to 140C 0.05C/min to 190C	190	5 µm	0.54 5.42	DNPH01 RDX-A213	4.45

Table A-III: Experiments with mixtures of RDX and DNPH

Experiment Name	Experiment Type	Type of Heating	Heating Rate (s)	Maximum Temp. °C	Orifice Diameter	Sample Size (mg)	Material	~ Residue Weight (mg)
	To Be Re-run (plugged orifice)							
DNPH028	Decomposition 1:10 ratio	Slow Ramp	2C/min to 140C 0.05C/min to 190C	190	2.9 µm	0.50 5.07	DNPH01 RDX-A213	4.4
DNPH029	Decomposition 1:10 ratio	Slow Ramp	2C/min to 140C 0.05C/min to 190C	190	5 µm	0.48 5.13	DNPH01 RDX-A213	5.02
	To Be Re-run (plugged orifice)							
DNPH030	Decomposition 1:10 ratio	Slow Ramp	2C/min to 140C 0.05C/min to 190C	190	5 µm		DNPH01 RDX-A213	
DNPH031	Decomposition 1:10 ratio	Slow Ramp	2C/min to 140C 0.05C/min to 190C	190	25.1 µm	~0.50 ~4.97	Aged DNPH01 Aged RDX-A213	2.89
DNPH032	Decomposition 1:10 ratio	Slow Ramp	2C/min to 140C 0.05C/min to 190C	190	24.8 µm	0.57 5.68	DNPH01 IRDX-02 SIRDX	3.93
DNPH033	Decomposition 1:10 ratio	Slow Ramp	2C/min to 140C 0.05C/min to 190C	190	24.0 µm	~0.51 ~5.12	Aged DNPH01 Aged SIRDX	3.76
DNPH034	Decomposition 1:10 ratio	Slow Ramp	2C/min to 140C 0.05C/min to 190C	190	24.0 µm	0.43 4.71	DNPH01 IRDX-03 IRDX	2.85
DNPH035	Decomposition 1:10 ratio	Slow Ramp	2C/min to 140C 0.05C/min to 190C	190	24.3 µm	~0.50 ~5.03	Aged DNPH01 Aged HIRDX	2.85
DNPH037	Decomposition 1:10 ratio	Slow Ramp	2C/min to 140C 0.05C/min to 190C	190	23.7 µm	0.53 5.24	DNPH01 IRDX-01 HIRDX	3.25

Table. 5. High Resolution Spectra of DNPH

Table B-I: Mass Spectra of DNPH				
m/z_value	*%_Signal*	*Stoichiometry*	*Measured mass*	*Theoretical mass*
18	0.53			
27	0.24	C2H3	27.022865	27.0229265
28	0.45	N2	28.005609	28.0055994
		CO	28.018193	28.0181755
29	0.24	N2H	29.013449	29.0134245
30	1.00	NO	29.997452	29.99744
31	0.13	N2H3	31.029083	31.0290745
32	0.34	O2	31.989286	31.9892807
		N2H4	32.036913	32.0368996
36	0.29			
38	0.11			
39	1.30	C3H3	39.023047	39.0229265
40	0.10	not seen		
41	0.12	C3H5	41.038642	41.0385766
42		C3H6	42.043609	42.0464016
43		C2H3O	43.017857	43.0178411
		C2H5N	43.041967	43.0416506
44	0.12	CO2	43.989374	43.9892807
45	0.24	C2H5O	45.033476	45.0334912
		CHO2	44.997233	44.9971057
46		NO2	45.992425	45.9923547
50	0.18	C4H2	50.015149	50.0151015
51	4.76	C4H3	51.022977	51.0229265
52	1.64	C3H2N	52.018214	52.0181755
		C4H4	52.030791	52.0307515
53	0.35	C3H3N	53.02605	53.0260005
		C4H5	53.039	53.0386
		C3HO	53.0023	53.0022
54	0.17	C3H4N	54.033681	54.0338256
55	0.12	C4H7	55.05423	55.0542266
		C3H3O	55.017782	55.0178411
63	0.27	C5H3	63.0229265	63.0229265
		C4HN	63.010344	63.0103505
64	0.52	C5H4	64.030787	64.0307515
		C4H2N	64.018099	64.0181755
65	0.22	C5H5	65.038633	65.0385766
		C4H3N	65.026174	65.0260005
66	0.67	C4H4N	66.033958	66.0338256
		C3H2N2	66.021056	66.0212495
67	0.15	C4H3O	67.018235	67.0178411

Table B-I: Mass Spectra of DNPH				
m/z_value	*%_Signal*	*Stoichiometry*	*Measured mass*	*Theoretical mass*
		C4H5N	67.041479	67.0416506
68	0.49	C3H2NO	68.013097	68.0130901
75	1.55	C6H3	75.022919	75.0229265
		C5HN	75.01052	75.0103505
76	1.57	C6H4	76.03075	76.0307515
		C5H2N	76.018292	76.0181755
77	1.77	C5H3N	77.026035	77.0260005
		C6H5	77.038536	77.0385766
78	8.23	C5H4N	78.033828	78.0338256
79	12.08	C5H3O	79.017827	79.0178411
80	1.07	H4N2O3	80.021406	80.0216434
		C4H2NO	80.013179	80.0130901
81	0.11	C3H3N3	81.032487	81.0321485
		C6H9	81.069716	81.0696769
82	0.13	in the noise		
90	0.15	C6H4N	90.033601	90.0338256
91	0.17	C6H5N	91.041578	91.0416506
92	2.04	C6H4O	92.025668	92.0256662
93	0.34	C5H5N2	93.044813	93.0447246
94	0.18	C5H4NO	94.02952	94.0287402
		C6H8N	94.065384	94.0651257
95	0.11	C4H3N2O	95.022739	95.0239891
104	0.20	noise		
105	0.68	C6H5N2	105.044675	105.0447246
		C6H3NO	105.021307	105.0209151
106	1.12	C6H4NO	106.028764	106.0287402
107	0.51	C6H5NO	107.036956	107.0365652
122	5.52	C6H4NO2	122.023636	122.0236548
123	0.42	* 13C C5H4NO2	123.027015	123.0270096
134	0.12	noise		
135	0.83	C6H5N3O	135.043658	135.0427132
136	0.34	noise		
137	0.13	C6H5N2O2	137.036086	137.0345538
150	0.19	not seen		
152	0.87	C6H4N2O3	152.022418	152.0216434
153	0.15	C6H5N2O3	153.030907	153.0294685
164	0.21	C6H4N4O2	164.031991	164.0328768
180	8.09	C6H4N4O3	180.027785	180.0277914
181	0.98	13C probably - otherwise not good id		
198	29.44	C6H6N4O4	198.03819	198.0383561
199	3.07	*13C C5H6N4O4	199.041658	199.041711

High Resolution Spectra from the Decomposition of DNPH.

Table B- II. Mass Spectra of DNPH Decomposition Products				
m/z_value	*%_Signal*	*Stoichiometry*	*Measured Mass*	*Theoretical Mass*
28	2.99	N2	28.00561	28.00560
29	0.15	N2H ?	29.01343	29.01342
		CHO	29.00240	29.00219
30	5.03	NO	29.99745	29.99744
31	0.25	Not seen		
32	0.68			
36	0.90	Noise		
38	0.30			
39	0.41	C3H3	39.02294	39.02293
41	0.15	C3H5	41.03860	41.03858
		C2H3N	41.02605	41.02600
42	0.16	C2H4N	42.03397	42.03383
43	0.14	C3H7	43.05425	53.05423
		C2H3O	43.01778	43.01784
44	0.41	CO2	43.98926	43.98928
		CH2NO	44.01289	44.01309
45	1.36	CHO2	44.99705	44.99711
46	0.14	NO2	45.99238	45.99235
51	0.85	C4H3	51.02294	51.02293
		C3HN	51.01362	51.01035
52	0.38	C3H2N	52.01819	52.01818
		C4H4	52.03077	52.03075
53	0.12	C3H3N	53.02600	53.02600
55	0.54	C3H3O	55.01787	55.01784
		C2H3N2	55.02909	55.02907
56	0.16	Noise		
57	0.41	C3H5O	57.33033	57.03349
59	0.15	Noise		
63	0.50	C5H3	63.02294	63.02293
		C4HN	63.01039	63.01035
64	0.88	C5H4	64.03077	64.03075
		C4H2N	64.01819	64.01818
65	0.49	C5H%	65.03865	65.03858
		C4H3N	65.02605	65.02600
66	0.17	C4H4N	66.03381	66.03383
		C3H2N2	66.02120	66.02125
67	0.14	C4H5N	67.04163	67.04165
		C3H3N2	67.02900	67.02907
68		C3H2NO	68.01309	68.01309
69	0.20	Not seen above noise around pftba peak		

Table B- II. Mass Spectra of DNPH Decomposition Products				
m/z_value	*%_Signal*	*Stoichiometry*	*Measured Mass*	*Theoretical Mass*
70	0.43	C3H4NO	70.02855	70.02874
71	0.41	Not seen		
72	0.13	Noise		
73		C3H5O2	73.02849	73.02841
75	1.86	C6H3	75.02295	75.02293
		C5HN	75.01026	75.01035
76	1.10	C6H4	76.03078	76.03075
		C5H2N	76.01824	76.01818
77	0.42	C5H3N	77.02602	77.02600
		C6H5	77.03860	77.03858
78	0.92	C5H4N	78.03384	78.03383
79	1.66	C5H3O	79.01786	79.01784
		N2H3O3	79.01365	79.01382
		C5H5N	79.04165	79.04165
80	0.48	C4H2NO	80.01313	80.01309
		N2H4O3	80.02117	80.02164
		C5H6N	80.04947	80.04948
81	0.25	Not seen		
82	0.19	Noise		
83	0.28	Not seen		
84	0.25	Not seen		
85	0.20	Noise		
90	0.22	C6H4N	90.03382	90.03383
91	0.38	C6H5N	91.04157	90.04165
		C5H3N2	91.02918	91.02907
92	3.47	C6H4O	92.02570	92.02567
93	0.32	C5H3NO	93.02102	93.02092
94	0.12	C5H4NO	94.02902	94.02874
95	0.23	C5H5NO	95.03678	95.03657
		C4H3N2O	95.02428	95.02399
96	0.24	Not seen		
97	0.42	Noise		
98	0.16	Noise		
99	0.23	Noise		
105	0.19	C6H5N2	105.04481	150.04472
		C6H3NO	105.02125	105.02092
106	0.53	C6H4NO	106..02880	
		C5H4N3	106.03991	106.03997
107	0.40	C6H5NO	107.03679	107.03657
108	0.38	C3H8O4	108.04150	108.04171
109	0.23	Noise		
110	0.26	Noise		
111	0.37	Noise		
112	0.51	Not seen		

Table B- II. Mass Spectra of DNPH Decomposition Products				
m/z_value	*%_Signal*	*Stoichiometry*	*Measured Mass*	*Theoretical Mass*
113	0.25	Noise		
119	0.18	C6HNO2	119.00105	119.00132
121	0.15	C6H5N2O	121.03914	121.03964
122	3.76	C6H4NO2	122.02373	122.02365
123	0.57	CH5N3O4	123.02778	123.02746
		C6H7N2O	123.05521	123.05529
124	0.24	Noise		
125	0.32	C5H5N2O2	125.03373	125.03455
126	0.14	Not seen		
127	0.30	Noise		
134	0.30	C6H4N3O	134.03488	134.03489
135	0.16	C6H5N3O	135.04249	135.04271
136	0.50	C6H4N2O2	136.02679	136.02673
137	0.29	C6H5N2O2	137.03415	137.03455
138	2.80	C6H6N2O2	138.04303	138.04352
139	0.45	Noise		
140	0.19	Noise		
141	0.21	Noise		
149	0.65	C8H5O3	149.02343	149.02332
150	0.20	C6H4N3O2	150.02977	150.02980
151	0.18	Noise		
152	0.47	C6H4N2O3	152.02166	152.02164
153	0.68	C6H5N2O3	153.02953	153.02947
		C6H7N3O2	153.05344	153.05328
154	0.24	Not seen		
155	0.18	noise		
164	2.60	C6H4N4O2	164.03300	164.30329
165	0.36	C6H5N4O2	165.03672	165.04070
166	0.16	Note seen		
167	0.61	C6H5N3O3	167.03386	167.03254
168	18.90	C6H4N2O4	168.01667	168.01656
169	1.50	C5HN2O5	169.98812	169.09880
170	0.25	Not seen		
179	0.10	Not seen		
180	0.76	C6H4N4O3	180.02787	180.02779
183	0.82	C6H5N3O4	183.02757	183.02746
184	0.34	C6H6N3O4	184.03248	184.03528
185	0.26	?C8H15N3O2	185.11725	185.11588
197	1.34	Not seen		
198	0.26	C6H6N4O4	198.03851	198.03840
199	0.33	C6H7N4O4	199.04402	199.04618
202	0.20	Noise		
207	0.13	Noise		
210	0.11	Noise		

Table B- II. Mass Spectra of DNPH Decomposition Products				
m/z_value	*%_Signal*	*Stoichiometry*	*Measured Mass*	*Theoretical Mass*
213	0.14	Noise		
217	0.11	Noise		
218	0.12	Not seen		
219	0.24	Noise		
221	0.21	Noise		
222	0.12	Noise		

Table. 6. High Resolution Spectra from the Decomposition of DNPH and RDX.

Table B-III. Mass Spectra of Products from Decomposition of DNPH and RDX				
m/z_value	%_Signal	Stoichiometry	Measured Mass	Theoretical Mass
28	4.79	N2	28.005567	28.0055994
		CH2N	28.018147	28.0181755
29	0.24	CH3N	29.02597	29.0260005
		CHO	29.002	29.002
		N2H	29.013	29.013
30	6.36	NO	29.997403	29.99744
31				
32	0.28	O2	31.989253	31.9892807
36	0.31			
38	0.10			
39	0.33	C3H3	39.022913	39.0229265
42	0.28	C2H4N	42.033812	42.0338256
		CH2N2	42.02125	42.0212495
43	0.28	CH3N2	43.029051	43.0290745
		C2H3O	43.017811	43.0178411
44	8.26	CH2NO	44.013066	44.0130901
		CO2	43.989243	43.9892807
45	0.98	CHO2	44.997093	44.9971057
46	0.73	NO2	45.992351	45.9923547
50		C4H2	50.015097	50.0151015
51	0.34	C4H3	51.022916	51.0229265
52	0.19	C3H2N	52.018167	52.0181755
54		C3H4N	54.033807	54.0338256
		C2H2N2	54.021278	54.0212495
55	0.22	C2H3N2	55.029058	55.0290745
		C3H3O	55.017834	55.0178411
56	0.24	C2H4N2	56.0369	56.0368996
		C2H2NO	56.013108	56.0130901
57	0.25			
62		C5H2	62.015107	62.0151015
63	0.20	C5H3	63.022927	63.0229265
64	0.81	C5H4	64.030756	64.0307515
65	0.12	C4H3N	65.02601	65.0260005
		C5H5	65.038567	65.0385766
68	0.15	C3H2NO	68.013062	68.0130901
		C3H4N2	68.036831	68.0368996
70	0.20	C3H4NO	70.028675	70.0287402
71	0.55	C2H3N2O	71.024003	71.0239891
74		C6H2	74.015111	74.0151015
		CH2N2O2	74.010634	74.0110787

Table B-III. Mass Spectra of Products from Decomposition of DNPH and RDX				
m/z_value	%_Signal	Stoichiometry	Measured Mass	Theoretical Mass
75	2.39	C6H3	75.022962	75.0229265
		CH3N2O2	75.018846	75.0189038
76	1.06	C6H4	76.03077	76.0307515
77	0.31	C5H3N	77.026017	77.0260005
78	0.34	C5H4N	78.033834	78.0338256
79	0.52	C5H3O	79.01785	79.0178411
80	0.27	C4H2NO	80.013114	80.0130901
		C5H6N	80.049468	80.0494756
		N2H4O3	80.02151	80.0216434
81	0.31	C3H3N3	81.032143	81.0321485
82	0.21	C3H4N3	82.039994	82.0399736
83	0.22	C3H5N3	83.047848	83.0477986
84	0.15			
85	0.17			
88		C6H2N	88.018153	88.0181755
89		C6H3N	89.025982	89.026000
		C7H5	89.038556	89.0385766
90		C6H4N	90.03384	90.0338256
91	0.16	C6H5N	91.041637	91.0416506
92	2.74	C6H4O	92.025688	92.0256662
93	0.28	CH5N2O3	93.029012	93.0294685
		C5H3NO	93.020923	93.0209151
		C5H5N2	93.044659	93.0447246
95	0.14	C5H5NO	95.03655	95.0365652
		C5H7N2	95.060265	95.0603747
		C4H3N2O	95.02401	95.0239891
96	0.14			
97	0.23	C4H5N2O	97.039544	97.0396392
		C6H9O	97.064834	97.0647913
98	0.25	C3H4N3O	98.034866	98.0348882
99	0.12			
101		C2H3N3O2	101.021912	101.0219778
102		C2H4N3O2	102.029845	102.0298028
105	0.12	C6H5N2	105.04475	105.0447246
106		C6H4NO	106.028788	106.0287402
107	0.22	C6H5NO	107.036642	107.0365652
110	0.15			
111	0.29	C4H3N2O2	111.018914	111.0189038
112	0.13			
113	0.12			
117		C7H5N2	117.044767	117.0447246
120	0.59	CH2N3O4	120.004068	120.003982
122	3.67	C6H4NO2	122.023716	122.0236548
123	0.43	C6H7N2O	123.055215	123.0552893

Table B-III. Mass Spectra of Products from Decomposition of DNPH and RDX				
m/z_value	%_Signal	Stoichiometry	Measured Mass	Theoretical Mass
		C3H7O5	123.02838	123.028799
124	0.13			
125	0.26	C5H5N2O2	125.034722	125.0345538
126	0.13			
127	0.29	C3H3N4O3	127.02521	127.0250518
128	0.81	C3H4N4O2	128.032929	128.0328768
132		C6N2O2	131.994605	131.9954287
133		C7H5N2O	133.039631	133.0396392
136		C6H4N2O2	136.02683	136.0267288
137	0.13			
138	0.61	C6H4NO3	138.01856	138.0185694
		C6H6N2O2	138.042433	138.0423789
139	0.19			
140	0.16			
141	0.14			
147		C7H5N3O	147.043085	147.0427132
		C2H3N4O4	147.014814	147.014881
148	0.27	C2H4N4O4	148.021121	148.0227061
149	0.22	C8H5O3	149.023649	149.0233204
150		C6H4N3O2	150.030088	150.0298028
151	0.12			
152	0.42	C6H4N2O3	152.021706	152.0216434
153	0.28	C6H5N2O3	153.029486	153.0294685
154	0.16			
155	0.11			
159	0.11			
163		C7H5N3O2	163.037732	163.0376278
164	0.13	C6H4N4O2	164.033385	164.0328768
165	0.39			
166	0.14			
167	0.35			
168	20.46	C6H4N2O4	168.01665	168.016558
169	1.63	13C C5H4N2O4	169.020108	169.0202694
170	0.23			
180	0.35	C6H4N4O3	180.027997	180.0277914
181	0.18			
182	0.10			
183	0.29	C6H5N3O4	183.027567	183.0274979
184	0.31	C6H4N2O5	184.010881	184.0114727
191	0.10			
197	0.63			
198		C6H6N4O4	198.038481	198.038397
205	0.16	C3H6N6O5	205.031898	205.0315937
209	0.11			

Table B-III. Mass Spectra of Products from Decomposition of DNPH and RDX				
m/z_value	%_Signal	Stoichiometry	Measured Mass	Theoretical Mass
210	0.97	C7H6N4O4	210.038458	210.038397
211	0.15			
218	0.11			
219	0.19			

Distribution

15 Commander, U.S. Army TACOM-ARDEC
Bldg. 3022
Picatinny Arsenal, NJ 07806-5000
ATTN: B. D. Fishburn AMSTA_AR_AEE-D

1 Commander, U.S. Army TACOM-ARDEC
Bldg. 3022
Picatinny Arsenal, NJ 07806-5000
ATTN: Sanjeev Singh AMSRD_AAR_WEE-W

1 Commander, U.S. Army TACOM-ARDEC
Bldg. 3022
Picatinny Arsenal, NJ 07806-5000
ATTN: Rao Surapaneni

1 Ruth Doherty
NSWC, Indian Head Division
101 Strauss Ave., Code 4210D
Indian Head, MD 20640

1 Michael Kramer
Arfl/Mnme
2306 Perimeter Road, Suite 9
Elgin, AFB, FL 32542-5910

1 Jon Maienschein
Lawrence Livermore National Lab,
Energetic Materials Section Chemistry
PO Box 800 L-282,
Livermore, CA 94550

1 Robert L. McKenney
Arfl/Mnme
2306 Perimeter Road, Suite 9
Elgin, AFB, FL 32542-5910

1 George Overturf
Lawrence Livermore National Lab,
Energetic Materials Section Chemistry
PO Box 800 L-282,
Livermore, CA 94550

1 Robert W. Shaw
Associate Director for Chemical Sciences
US Army Research Office
4300 South Miami Blvd.
Box 12211
Research Triangle Park, NC 27709-2211

1 Al Stern
NSWC, Indian Head Division
101 Strauss Ave., Code 4210D
Indian Head, MD 20640

1 Chris Walsh
Advanced Gun Propellant Development Program Manager
NSWC, Indian Head Division
101 Strauss Ave., Code 4210D
Indian Head, MD 20640

10 MS9052 Richard Behrens, 08368
1 MS9052 Lois Johnston, 08368
1 MS9052 Deneille Wiese-Smith, 08368
1 MS9052 Sean Maharrey, 08368
1 MS9054 Jessica Matto, 08350
1 MS9052 Aaron Highley, 08368
3 MS9018 Central Technical File, 8945-1
1 MS0899 Technical Library, 9616
1 MS9021 Classification Office, 8511 for Technical Library, MS 0899, 9616

1 MS9054 Bill McLean, 08300
1 MS 9054 Bob Carling, 08350
1 MS9054 Don Hardesty, 08360
1 MS9054 Dave Chandler, 08350
1 MS9054 Larry Rahn, 08350
1 MS9051 Andrew McIlroy, 08351
1 MS9055 Sarah Allendorf, 08353
1 MS9951 Art Pontau, 08358
1 MS9053 Dennis Siebers, 08362
1 MS9052 Jay Keller, 08367
1 MS9056 Wen Hsu, 08368
1 MS9005 Russ Miller, 08230
1 MS9004 Rick Stulen, 08100
1 MS9007 Doug Henson, 08200
1 MS9405 Jill Hruby, 08700
1 MS9007 Ming Lau, 08201
1 MS9005 Greg Thomas, 08220
1 MS9034 Al McDonald, 08221
1 MS 9035 Bill Wilson, 08230
1 MS9005 Brian Damkroger, 08240
1 MS9404 Glen Kubiak, 08750
1 MS9161 Bill Even, 08760
1 MS9403 Tim Shepodd, 08762
1 MS9161 E. P. Chen, 08763
1 MS9405 Ken Wilson, 08770
1 MS9402 Chuck Cadden, 08772
1 MS9403 Jim Wang, 08773
1 MS9042 Paul Spence, 08774
1 MS0151 Tom Hunter, 09000

1 MS9001 Mim John, 08000
1 MS0457 John Stichman, 02000
1 MS1427 Julia Phillips, 01100
1 MS0887 Michael Cieslak, 01800
1 MS0885 Richard Salzbrenner, 01801
1 MS0887 Michael Cieslak, 01800
1 MS0885 Richard Salzbrenner, 01801
1 MS0889 Jeff Braithwaite, 01861
1 MS0512 Thomas Blejwas, 02500
1 MS0521 Michael Prairie, 02520
1 MS0521 Corey Knapp, 02560
1 MS1453 Wendy Cieslak, 02550
1 MS1452 Steven Harris, 02552
1 MS1453 Gregory Scharrer, 02253
1 MS1454 Lloyd Bonzon, 02554
1 MS1455 Leanna Minier, 02555
1 MS1454 Anita Renlund, 02554
1 MS1454 Michael Kaneshige, 02554
1 MS1454 Alex Tappan 02554
1 MS0151 Art Ratzel, 09750
1 MS0836 Gene Hertel, 09116
1 MS0836 William Erikson, 09116
1 MS0836 Robert Schmitt, 09116